SPC Mesoscale Analysis Compared to Field-Project Soundings: Implications for Supercell Environment Studies

MICHAEL C. CONIGLIO[a,b] AND RYAN E. JEWELL[c]

[a] *NOAA/National Severe Storms Laboratory, University of Oklahoma, Norman, Oklahoma*
[b] *School of Meteorology, University of Oklahoma, Norman, Oklahoma*
[c] *NOAA/Storm Prediction Center, Norman, Oklahoma*

(Manuscript received 23 August 2021, in final form 8 December 2021)

ABSTRACT: A total of 257 supercell proximity soundings obtained for field programs over the central United States are compared with profiles extracted from the SPC mesoscale analysis system (the SFCOA) to understand how errors in the SFCOA and in its baseline model analysis system—the RUC/RAP—might impact climatological assessments of supercell environments. A primary result is that the SFCOA underestimates the low-level storm-relative winds and wind shear, a clear consequence of the lack of vertical resolution near the ground. The near-ground (≤500 m) wind shear is underestimated similarly in near-field, far-field, tornadic, and nontornadic supercell environments. The near-ground storm-relative winds, however, are underestimated the most in the near-field and in tornadic supercell environments. Underprediction of storm-relative winds is, therefore, a likely contributor to the lack of differences in storm-relative winds between nontornadic and tornadic supercell environments in past studies that use RUC/RAP-based analyses. Furthermore, these storm-relative wind errors could lead to an under emphasis of deep-layer SRH variables relative to shallower SRH in discriminating nontornadic from tornadic supercells. The mean critical angles are 5°–15° larger and farther from 90° in the observed soundings than in the SFCOA, particularly in the near field, likely indicating that the ratio of streamwise to crosswise horizontal vorticity is often smaller than that suggested by the SFCOA profiles. Errors in thermodynamic variables are less prevalent, but show low-level CAPE to be too low closer to the storms, a dry bias above the boundary layer, and the absence of shallow near-ground stable layers that are much more prevalent in tornadic supercell environments.

SIGNIFICANCE STATEMENT: A total of 257 radiosonde observations taken close to supercell thunderstorms during field programs over the last 25 years are compared with a model-based analysis system (the SFCOA), which is often used for studying supercell thunderstorm environments. We present error characteristics of the SFCOA as they relate to tornado production and distance to the storm to clarify interpretations of environments favorable for tornado production made from past studies that use the SFCOA. A primary result is that the SFCOA underpredicts the speed and shear of the air flowing toward the storm in many cases, which may lead to different interpretations of variables that are most important for discriminating tornadic from nontornadic supercell thunderstorms. These results help to refine our understanding of the conditions that support tornado formation, which provides guidance on environmental cues that can improve the prediction of supercell tornadoes.

KEYWORDS: Storm environments; Radiosonde/rawinsonde observations; Model evaluation/performance; Supercells; Tornadoes

1. Introduction

An important component of understanding and predicting supercells is their interaction with the environment, which remains an active area of research (e.g., Coffer et al. 2019, 2020; Coniglio and Parker 2020; Flournoy et al. 2021; Goldacker and Parker 2021; Nixon and Allen 2021). Studies exploring how supercell behavior relates to their environment are plentiful and date back several decades, with more recent studies elucidating potential storm–environment feedbacks (Potvin et al. 2010; Parker 2014; Nowotarski and Markowski 2016; Wade et al. 2018; Kerr et al. 2019; Coniglio and Parker 2020; Flournoy et al. 2020). Estimates of the environment for these studies have been made from a variety of sources, from rawinsonde observations (Kerr and Darkow 1996; Rasmussen and Blanchard 1998; Rasmussen 2003; Parker 2014; Wade et al. 2018; Coniglio and Parker 2020), remote sensing (Wagner et al. 2008; Botes et al. 2012), to three-dimensional analyses produced from blends of available observations and numerical models (e.g., Markowski et al. 2003; Thompson et al. 2003; Togstad et al. 2011; Smith et al. 2012; Thompson et al. 2012; Nowotarski and Jensen 2013; Coffer et al. 2019, 2020; Goldacker and Parker 2021; Nixon and Allen 2021, among others).

Gridded analyses allow for much more frequent diagnosis of the environment in proximity to convection than routine rawinsonde observations. One analysis system that has been used widely for storm environment studies is the Rapid Refresh [RAP; or Rapid Update Cycle (RUC) prior to 2012]. For three decades, the RUC/RAP has provided a gridded, hourly updated synthesis of routinely available observations describing current environmental conditions. Variables derived from these analyses have been shown to

Corresponding author: Michael C. Coniglio, michael.coniglio@noaa.gov

DOI: 10.1175/MWR-D-21-0222.1

provide skillful forecast guidance through discrimination of nontornadic and tornadic supercells (e.g., Thompson et al. 2003, 2012; Coffer et al. 2019).

A flavor of the RUC/RAP analysis used in both operational forecasting and in storm–environment studies is the SPC mesoscale surface objective analysis (SFCOA). For the SFCOA near-surface variables, the gridded RUC/RAP analysis of 2-m temperature and humidity, as well as 10-m wind, are replaced with a two-pass Barnes analysis of current surface observations. Although the main purpose of this procedure was to incorporate the latest observations into a real-time mesoscale analysis system (Bothwell et al. 2002), this procedure also is used to produce an analysis of record archived at SPC, in which a Barnes analysis of the full surface observation dataset provided in the operational data stream replaces the final RUC/RAP surface analysis and is produced on a 40-km grid with 36 pressure levels (every 25 hPa). It is this 40-km version that is widely used in most of the model analysis-based storm–environment studies cited above. For earlier versions of this system, this analysis of record has been shown to produce somewhat smaller mean errors in most base-state and severe weather–related variables relative to the RUC/RAP base analysis (and relative to 1-h RUC/RAP forecasts in particular) (Coniglio 2012), but this evaluation is now a decade old. For newer versions of the SFCOA, Coffer et al. (2019) hinted at potential inadequacies in resolving the near-ground wind profiles and the consequences for determining near-ground storm-relative helicity (SRH). They also showed that mean winds, even well above the surface, can be several meters-per-second too slow when compared with VORTEX2 soundings (see their Fig. A1). Therefore, an updated comprehensive evaluation of the SFCOA seems warranted given the frequent upgrades of the RUC/RAP and its wide use in storm–environment studies.

Recently, Coniglio and Parker (2020, hereinafter CP20) compiled several hundred rawinsonde observations taken near supercells over three decades and 13 field projects to examine storm–environment relationships. The CP20 dataset includes rawinsonde observations from 1994 to 2019 and can be utilized to provide an updated estimate of the accuracy and error characteristics of the SFCOA for the purpose of refining our knowledge of supercell–environment relationships. A particular motivation for this study comes from apparent discrepancies in variables that discriminate nontornadic and tornadic supercells in CP20 relative to other studies that use the SFOCA and RUC/RAP analyses. A primary result from CP20 are significant differences in both low- and midlevel storm-relative winds between nontornadic and tornadic soundings. This is intriguing for two reasons: 1) the dynamical importance of storm-relative winds for supercells has received renewed attention in recent years (e.g., Warren et al. 2017; Peters et al. 2020), and 2) differences in storm-relative winds between nontornadic and tornadic supercells are not seen in many past studies that use RUC/RAP-based profiles (e.g., Thompson et al. 2003; Markowski et al. 2003; Nowotarski and Jensen 2013; Coffer et al. 2019). Another discrepancy is that the angle of the near-ground shear vector relative to storm motion (i.e., the critical angle[1]) is larger and farther from 90° in CP20 relative to past studies that use RUC/RAP-based datasets. The critical angle is often used as an estimate of the amount of near-ground streamwise horizontal vorticity in the environment, which factors largely into the tornadic potential of supercells (Coffer and Parker 2017), thus the accuracy of near-ground wind analyses is important to understand. The purpose of this study is to examine the role that errors in the RUC/RAP fields might play in the above discrepancies. More broadly, this study will also serve to quantify the general error characteristics of the 40-km (25 hPa) version of the SFCOA in supercell environments. Since a version of the SFCOA based on 1-h RUC/RAP forecasts is used widely in operational forecasting (https://www.spc.noaa.gov/exper/mesoanalysis/), differences could also reveal potential pitfalls in forecast applications that use this dataset.

2. Data and methods

Up to 1 May 2012, the background 3D analysis for the SFCOA was provided by the RUC model (Benjamin et al. 2004a,b) after which the RAP model (Benjamin et al. 2016; Hu et al. 2017) was used. Over this period, the native RUC/RAP grid decreased in horizontal grid spacing from 20 km in 2002 to 13 km in 2005 and thereafter.[2] The SFCOA dataset evaluated here is archived at the SPC and available (nominally) every hour from 2003 to the present with data postprocessed on 25-hPa levels on a 40-km grid (hereinafter this archive is referred to simply as the SFCOA for brevity). Although the SFCOA has been produced occasionally on 20-km grids, the available period of this version is much shorter. Of particular concern here is the accuracy of the SFCOA near the ground.[3] There are only three levels below 500 m in the SFCOA, with only 5–6 levels below 500 m in the native RUC/RAP hybrid-sigma levels (there were 50 total vertical levels in the RUC prior to 2005, and 51 levels thereafter; Benjamin et al. 2016). Although analyses using these RUC/RAP native levels would add some vertical resolution, there are no comprehensive climatological studies that use the RUC/RAP native levels to the authors' knowledge, and thus we limit the present study to an analysis of the SFCOA.

The rawinsonde observations (raobs) used in this study is described in detail in CP20 and overlaps in time with the SFCOA from 2003 to 2019. These raobs were obtained from field programs near supercells and underwent extensive quality control (see CP20 for details). This study focuses on the

[1] The critical angle was introduced in Esterheld and Giuliano (2008) and estimates the ratio of near-ground streamwise to crosswise horizontal vorticity by computing the angle between the 10–500-m vertical wind shear vector and the storm motion vector. An angle of 90° likely indicates large streamwise horizontal vorticity relative to crosswise horizontal vorticity in the lowest 500 m, but it is only an approximation of the 0–500-m streamwise horizontal vorticity.

[2] See Benjamin et al. (2016) for a detailed description of how the RUC evolved into the RAP and http://https://rapidrefresh.noaa.gov/ for further developments since 2016.

[3] Hereinafter, near ground refers to levels ≤500 m.

raobs taken from 10 to 120 km of the supercell updraft and are gathered from a sector generally east and south of the supercell (in a framework where east aligns with the supercell motion vector) acting as proxy observations for the supercell's mesoscale environment, or what is considered "truth." As in CP20, only those soundings with positive 0–3-km lowest 100-hPa mixed-layer CAPE (CAPE03) are included here to exclude those excessively influenced by the storm's cold pool or that did not sample the proximate unstable air mass (e.g., it sampled the dry side of a dryline). We further require that raobs have data gaps no larger than 100 m up to at least 3 km AGL[4] to ensure the resolution advantage of the raobs relative to the SFCOA is maintained. The raobs taken within 10 km of the updraft are removed from the analysis because they usually enter the updraft, effectively sampling the storm itself (seven others that enter the updraft from more than 10 km away also are removed). See CP20 for how the storm updraft was identified.

The inclusion of raobs from as close as 10 km away from the updraft will presumably allow for storm-induced modification to the ambient environment to be included in the analysis (Potvin et al. 2010). Although the RUC/RAP has long attempted to incorporate at least some effects of convection into the analysis by introducing latent heating, cloud, and hydrometeors during the digital filter initialization (Weygandt and Benjamin 2007; Benjamin et al. 2016), these adjustments likely do not capture the full storm- to meso-γ-scale modifications to the environment because convective motions do not occur on the native 13- or 20-km grids (this is explored later in this study). A version of the RAP run on a 3-km grid [the High-Resolution Rapid Refresh (HRRR)] has been run operationally since 2014 and has been in development since 2007 (see Benjamin et al. 2016 and https://rapidrefresh.noaa.gov/hrrr/). Although the convection-allowing grid spacing of the HRRR provides an opportunity to analyze storm- to meso-β-scale modifications in the near-storm environment, climatological storm–environment studies that use the HRRR analysis fields (e.g., Katona et al. 2016) are scarce in comparison with those that use RUC/RAP-based analyses, likely because the period of available data is still relatively short. For this reason, we do not include HRRR-analysis soundings here [although future work should follow Kerr et al. (2019) to explore how well near-storm environments are analyzed in convection-allowing modeling systems].

As shown later, SFCOA errors in some variables increase with decreasing distance to the storm. The near-storm environment may be modified by external factors, e.g., by preexisting outflow boundaries (Rasmussen et al. 2000; Hanft and Houston 2018) or by neighboring storms, but a primary reason for these modifications is likely storm-induced feedbacks from the storm itself. Low pressure perturbations very near the storms induced by latent heating and flow perturbations (especially from storm rotation; Weisman and Rotunno 2000; Davies-Jones 2002) are known to accelerate the nearby flow radially inward toward the storm (Parker 2014; Wade et al. 2018). Furthermore, modifications in the surrounding thermodynamic field can occur from diabatic heating/cooling

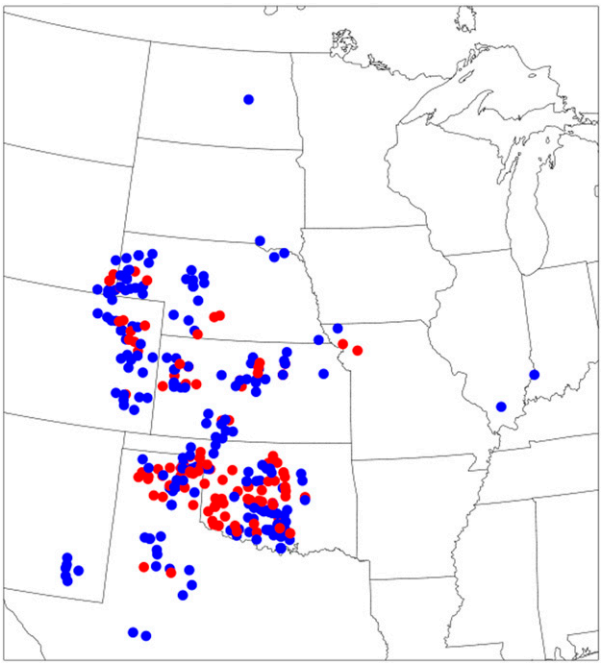

FIG. 1. Locations of the 257 raobs used in this study. A red dot indicates that a tornadic supercell was sampled between 6 min prior to and 90 min after the release of the rawinsonde, and a blue dot indicates that a nontornadic supercell was sampled.

(Nowotarski and Markowski 2016; Trapp and Woznicki 2017; Kerr et al. 2019). Although the spatial extent of these storm–environment feedbacks is likely a function of storm maturity and other factors (Potvin et al. 2010; Nowotarski and Markowski 2016; Trapp and Woznicki 2017; Wade et al. 2018; Kerr et al. 2019), these studies show that substantial modifications to the environment generally fall within 40 km of the storm; and so to help summarize these differences, we define the near-field storm inflow to be within 10–40 km of the updraft and the far field to be 40–120 km from the updraft following (Potvin et al. 2010) and CP20.

Furthermore, we will show important differences in SFCOA errors between a set of 143 raobs that sampled near a supercell that was never tornadic (hereinafter the NONTOR subset) and a set of 114 raobs that sampled near a supercell that produced an F/EF0+ (Fujita/enhanced Fujita scale) tornado between 6 min prior to and 90 min after the raob release (hereinafter the TOR subset). As detailed in CP20, the times and occurrences of tornadoes was determined using the SPC tornado database, which has a higher standard of quality control than does *Storm Data* (Smith et al. 2012). Subsets containing 75 NONTOR raobs and 62 TOR raobs in the far field (resulting in 137 total far-field raobs) and 68 NONTOR raobs and 52 TOR raobs in the near field (resulting in 120 near-field raobs) are compared. In total, the dataset has 257 raobs sampled from 105 separate storms over 66 unique days. Note that all of these raobs sampled central U.S. supercell environments (Fig. 1) and occurred between April and July with all but 12 occurring

[4] Hereinafter, all references to height are AGL.

TABLE 1. Description of severe weather–related variables computed from the soundings.

Acronym	Meaning
ANG or AZI	Angle (°) between storm motion and azimuth of the sounding relative to the updraft (see Fig. 9 for the convention)
DIST	Distance (km) of the near-ground location of the sounding to the updraft
TIME	UTC time of the sounding when near ground (launch time for upsondes; crash time for dropsondes)
CAPE##	Convective available potential energy (J kg^{-1}) using a lowest-100-hPa mixed parcel over the lowest 3 km (## = 03), the lowest 6 km (## = 06), and the lowest 10 km (## = 10)
MLCIN	Convective inhibition (J kg^{-1}) using a lowest-100-hPa mixed parcel
LR####	Temperature lapse rate (C km^{-1}) over the lowest 100 m (#### = 0100), 250 m (#### = 0250), 500 m (#### = 0500), 1 km (#### = 01KM), 3 km (#### = 03KM), and 700–500 hPa (#### = 7500)
LLMIX	0–1-km mean mixing ratio (g kg^{-1})
MLLCL	Lifting condensation level (m) using a lowest-100-hPa mixed parcel
GWS###	Ground-relative wind speed (m s^{-1}) at 10 m (## = 10), 100 m (### = 100), 250 m (### = 250), 500 m (### = 500), 1 km (### = 1km), 2 km (### = 2km), and 3 km (### = 3km)
SRW###	Mean storm-relative wind speed (m s^{-1}) at 10 m (## = 10), 100 m (## = 100), 250 m (### = 250), 500 m (### = 500), 1 km (### = 1km), 2 km (### = 2km), and 6 km (### = 6km)
SH####	Bulk wind difference (m s^{-1}) (vertical wind shear proxy) over the lowest 100 m (#### = 0100), 250 m (#### = 0250), 500 m (#### = 0500), 1 km (#### = 01KM) and 6 km (#### = 06KM)
CA####	Critical angle: acute angle (°) between the 10-m storm-relative wind and the shear vector over the lowest 100 m (#### = 0100), 250 m (#### = 0250), and 500 m (#### = 0500)
SRH####	Storm-relative helicity (m^2 s^{-2}) between 100 m (#### = 0100), 250 m (#### = 0250), 500 m (#### = 0500), 1 km (#### = 01KM) and 3 km (#### = 03KM)
EFFSH	Effective bulk wind difference (m s^{-1}) (Thompson et al. 2007)
EFFSRH	Effective storm-relative helicity (m^2 s^{-2}) (Thompson et al. 2007)
STP	Significant tornado parameter modified from (Thompson et al. 2012) to use CAPE06 or CAPE10 when MLCAPE is not available

in May and June, so the results presented here may not apply to other parts of the United States or in other seasons. Furthermore, the observed cases here are biased toward robust supercells that were the subject of most of the field projects from which the soundings were taken. Other studies of this type with larger sample sizes (e.g., Thompson et al. 2003; Coffer et al. 2019) likely represent a larger spectrum of supercell strengths and types.

The SFCOA and raob profiles are compared directly through mean error (ME) and mean absolute error (MAE) profiles (error is defined as the SFCOA value minus the raob value). ME represents the SFCOA bias, whereas MAE is a measure of the accuracy without regard to the direction of the over or underprediction. A direct comparison of the SFCOA and raob profiles requires interpolating the SFCOA base-state variables (temperature, dewpoint, and u- and v-wind components) to the observation location from the surrounding grid points. Three methods were explored: 1) a nearest-neighbor approach in which the profile comes from the grid point closest to the raob release location, 2) a Gaussian interpolation approach in which the profile is interpolated in space and time to the location of the raob release, and 3) as in 2) except to the location and time of the ascending upsonde (or descending dropsonde) to incorporate sonde drift. There were negligible differences in the results between all three methods, perhaps not surprising given the 40-km grid spacing of the SFCOA. The results presented hereinafter use SFCOA profiles generated using method 2 above to maintain some consistency in how profiles are typically extracted from mesoscale analysis systems. Since a goal of this study is to examine the impacts of low vertical resolution near the ground, the SFCOA profiles are interpolated (linearly) to 10-m levels between 0 and 6 km—the same as done for the raobs—prior to compositing.[5] The raobs have data every ~5 m and can presumably resolve features with length scales down to tens of meters. Therefore, the upscaled SFCOA profiles on 10-m levels provide a means to quantify the impacts of the stark difference in vertical resolution between the SFCOA and raob profiles.

In addition to error profiles, mean errors and select error distributions in severe weather–related variables are examined (see Table 1 for a description of these variables). As shown in CP20, the raob dataset used here shows significant differences between the NONTOR and TOR subsets that are not seen in other studies. In contrast to Thompson et al. (2003), Markowski et al. (2003), Nowotarski and Jensen (2013), and Coffer et al. (2019) (see Fig. 3 in Coffer et al. 2020), CP20 find significantly stronger low-level storm-relative[6] winds (SRWs) in the TOR subset. Furthermore, CP20 find critical angles (CAs) to be much larger than those shown in Coffer et al. (2019) and farther

[5] Converting to height AGL levels mitigates problems with mismatches between elevations in the interpolated SFCOA profiles and the observations. However, because most of the soundings used in this study were away from complex terrain, mismatches are generally small—82% of the soundings have surface pressure differences <5 hPa.

[6] Winds are converted to a storm-relative coordinate system with the observed storm motion aligned with the x axis and the storm motion at the origin (see CP20 for how observed storm motion was determined). The observed storm motion is used for computing both the SFCOA and raob storm-relative winds.

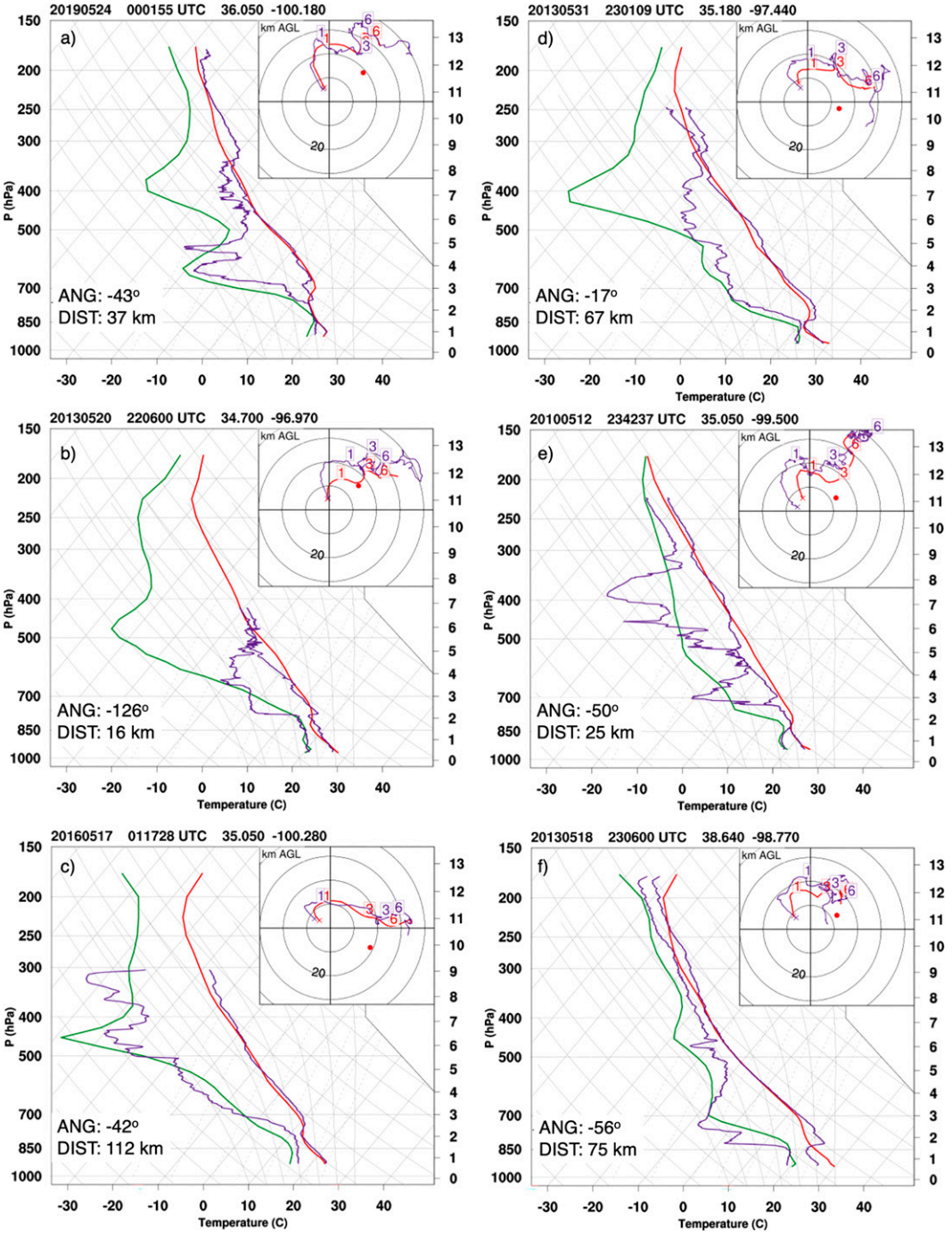

FIG. 2. Sounding comparisons between the SFCOA and raob profiles. SFCOA is in red–green and the raob is in purple. On the hodographs, heights are labeled at 1, 3, and 6 km AGL with range rings every 10 m s^{-1}. The observed storm motion is shown by the red dot. The date and times (UTC) for the raob release are shown at the top left in year-month-day hour-minute-second format along with the latitude and longitude. The azimuth (ANG) and distance (DIST) of the sounding release location in a storm-relative reference frame (with 0° pointing along storm motion and −90° pointing normal and to the right of storm motion) are provided in each panel.

from 90° for the *tornadic* supercells. CP20 suggested that some of these differences could be related to the use of RUC/RAP soundings in those studies instead of high-resolution raobs. The contribution to these discrepancies from the use of the RUC/RAP-based datasets is examined in this study.

Statistical significance in mean differences is assessed using a Welch's *t* test (which assumes unequal variance in subsets)

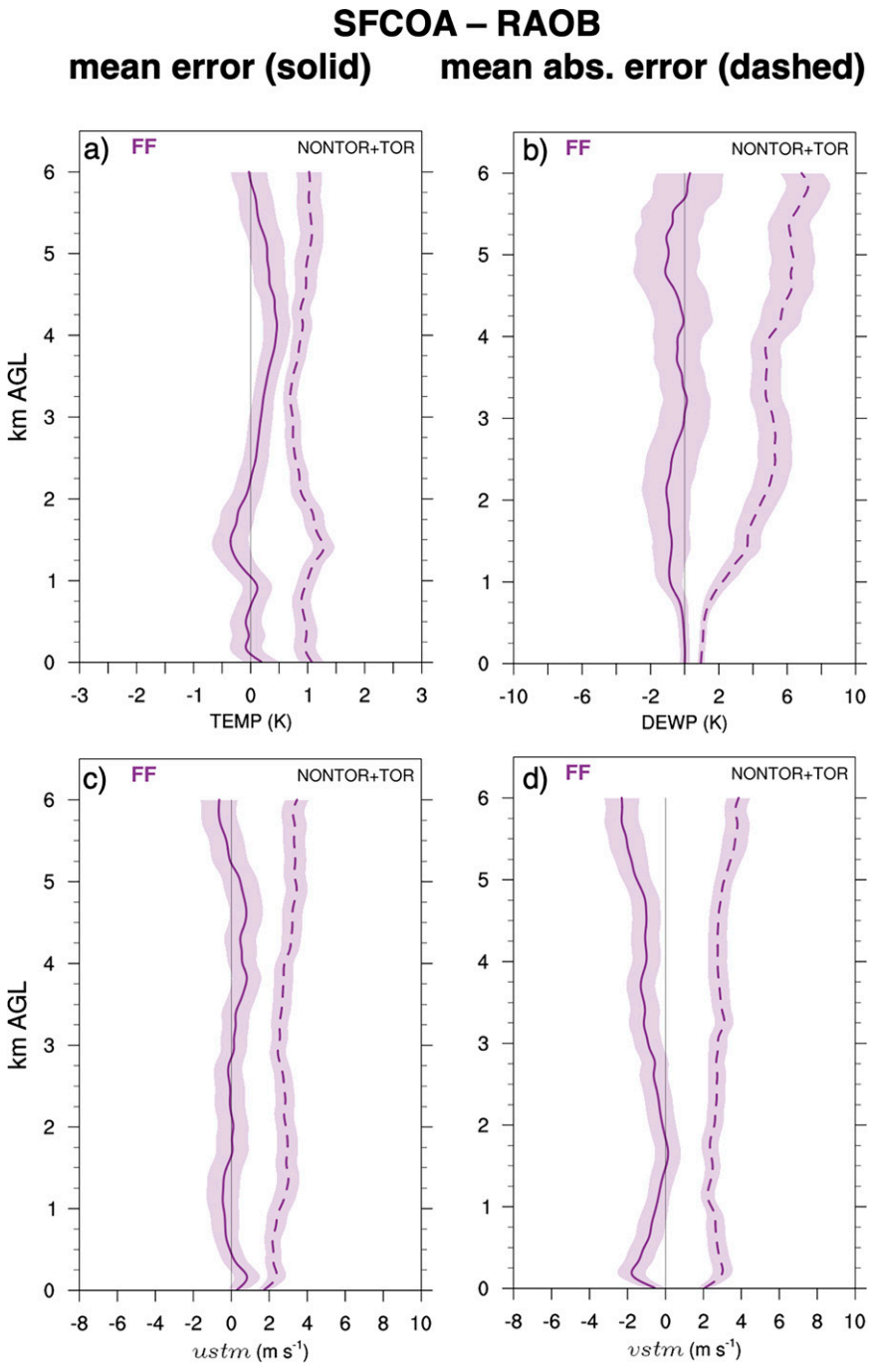

FIG. 3. Profiles of far-field (FF) SFCOA mean errors (solid) and mean absolute errors (dashed) up to 6 km AGL for the combined NONTOR and TOR subsets for (a) temperature (K), (b) dewpoint (K), and the (c) storm-relative wind component along storm motion (ustm) and (d) storm-relative wind component normal to storm motion (vstm) in meters per second.

with the number of unique *days* in each subset as the effective sample size. The number of days is used because multiple soundings and storms often occur on a single day in close proximity, and using those counts could violate the assumption of independent samples.

3. Results

Prior to describing the aggregate results, six individual comparisons of SFCOA and raob profiles are shown in Fig. 2. All of these examples show reasonably accurate analyses in some

aspects and inaccurate in others. Figure 2a shows an example with small SRH errors but large errors in the 4–6-km winds. Figure 2b shows similar errors in the 4–6-km winds and near-ground wind shear that is vastly underestimated. Figures 2a–c show soundings that contribute to the dry bias above the boundary layer discussed later. Figures 2d and 2e show large SRH errors but relatively small errors in boundary layer temperature and dewpoint. Figure 2f shows a large error in the CA and SRH, as well as a substantial error in the strength of the capping inversion. The results below summarize the characteristics of these errors in the entire dataset.

a. Far-field error profiles

An assessment of the SFCOA errors needs to carefully consider the potential influence of the storm on its environment. But first, we consider only the 137 raobs taken in the far field (NONTOR and TOR soundings combined) to minimize the storm-induced influences on the analysis for now (Fig. 3). In the far field, temperature errors (Fig. 3a) are generally small, with MAEs of only 0.5–1.5 K from the surface through 6 km. MEs in temperature are likewise small (all <0.5 K) but there is evidence of a small cool bias from 1 to 2 km and a small warm bias from 2.5 to 5 km. Consistent with Benjamin et al. (2004b), Coniglio (2012), and Evans et al. (2018), humidity MAEs grow larger from the surface to the middle troposphere (Fig. 3b). MAEs in dewpoint increase from about 1 K at the surface to almost 7 K at 6 km. Dewpoint MEs are close to zero in the lowest 500 m but show a dry bias of 1–2 K in the 1–2.5-km layer.

For the SRW, errors in the component along storm motion (ustm) are small, with ME magnitudes all <1 m s^{-1} and MAEs of around 2 m s^{-1} near the ground that increase to 3 m s^{-1} at 6 km. Errors in the component normal to storm motion (vstm) are larger, with a clear slow bias below 1 km and again above 3 km. The vstm MEs peak near 250 m with a value near -2 m s^{-1} and then peak again with a value near -2 m s^{-1} at 6 km. MAEs in vstm are 2–3 m s^{-1} near the ground and increase to near 4 m s^{-1} at 6 km.

Composite soundings and hodographs for the far-field subset (for the combined NONTOR and TOR subsets), and means of severe weather–related variables, are compared in Fig. 4. The composite far-field soundings reflect the small temperature errors and the slight dry bias in the 850–700-hPa layer. The slow bias in vstm is reflected in raob hodographs that are somewhat larger than the SFCOA hodographs below 1 km and again between 3 and 6 km (Fig. 4). The former results in significant differences (>95%) in the mean near-ground vertical wind shear (see SH0100, SH0250, and SH0500). For example, the mean 0–100-m shear increases from 2.2 m s^{-1} for the SFCOA to 4.6 m s^{-1} for the raobs, an increase of 113%. These errors could be related to deficiencies in depicting the effects of surface drag on near-ground variables. Evidence for this comes from 100- to 250-m *ground-relative* winds that are substantially stronger in the raobs (see GWS0100 and GWS0250 on Fig. 4). These errors are a clear indication of the inability of the RUC/RAP to depict the often large near-ground winds and wind shear in supercell environments (regardless of distance from the storm).

The NONTOR and TOR soundings contribute to the far-field errors similarly (Figs. 5 and 6). One exception is for the far-field near-ground lapse rates—errors are much larger for the TOR soundings than the NONTOR soundings. For example, the mean LR0250 for the far-field NONTOR soundings is 8.4 K km^{-1} in both the SFCOA and raobs (Fig. 5), but for the far-field TOR soundings, the mean LR0250 decreases from 9.0 K km^{-1} in the SFCOA to 6.9 K km^{-1} in the raobs (Fig. 6). Without accompanying satellite, surface mesonet, and radar observations near the ground, it is impossible to confidently prescribe reasons for these shallow stable layers and why they are preferentially seen in the TOR raobs. Differences in radiational cooling associated with the diurnal cycle are not to blame because differences in the time of day/year between the NONTOR and TOR subsets are negligible. Differences in anvil shading are one possible explanation. Exploring these differences is beyond the scope of this study, but is a topic for future research to examine if the anvil shading effects on near-ground wind shear explored in Nowotarski and Markowski (2016) could be playing a role.

The SRH over all layers examined also has larger errors in the far field for the TOR soundings than for the NONTOR soundings. The near-ground wind shear errors, along with SRWs that are too slow, contribute to these SRH values that are too low. For example, the mean SRH0500 is only 9 m^2 s^{-2} higher (from 72 to 81 m^2 s^{-2}, or 12%) in the raobs for the NONTOR soundings (Fig. 5), but increases 38 m^2 s^{-2} (from 119 to 157 m^2 s^{-2}, or 32%) in the raobs for the TOR soundings (Fig. 6). These larger SRH errors in the far-field TOR soundings are not limited to the near-ground layers. For example, the mean EFFSRH is only 19 m^2 s^{-2} higher (from 184 to 203 m^2 s^{-2}, or 9%) in the raobs for the NONTOR soundings (Fig. 5), but increases 79 m^2 s^{-2} (from 278 to 357 m^2 s^{-2}, or 29%) for the TOR soundings (Fig. 6). It is difficult to say what practical difference these larger errors may make in an operational setting, but mean errors in SRH0500 near -40 m^2 s^{-2} and EFFSRH near -80 m^2 s^{-2} are quite large relative to the range of values typically analyzed for these variables in supercell environments (Thompson et al. 2007; Coffer et al. 2019).[7] Recognizing that the values stated in the previous sentence are *mean* errors, meaning errors are often larger than those values stated (distributions of these errors are shown later), the use of the SFCOA could often lead to a substantial underestimation of the tornadic potential in the environment.

[7] For reference, (Thompson et al. 2007) find median EFFSRH values to increase from about 100 m^2 s^{-2} for nontornadic supercells, to 150 m^2 s^{-2} for weakly tornadic supercells, to 230 m^2 s^{-2} for significantly tornadic supercells (values are estimated from their Fig. 8). (Coffer et al. 2019) show median values of SRH0500 to vary from 64 m^2 s^{-2} for the nontornadic supercells, to about 130 m^2 s^{-2} for the weakly tornadic supercells, to 224 m^2 s^{-2} for the significantly tornadic supercells (values for the weakly tornadic supercells are estimated from their Fig. 2). Both studies use the SFCOA.

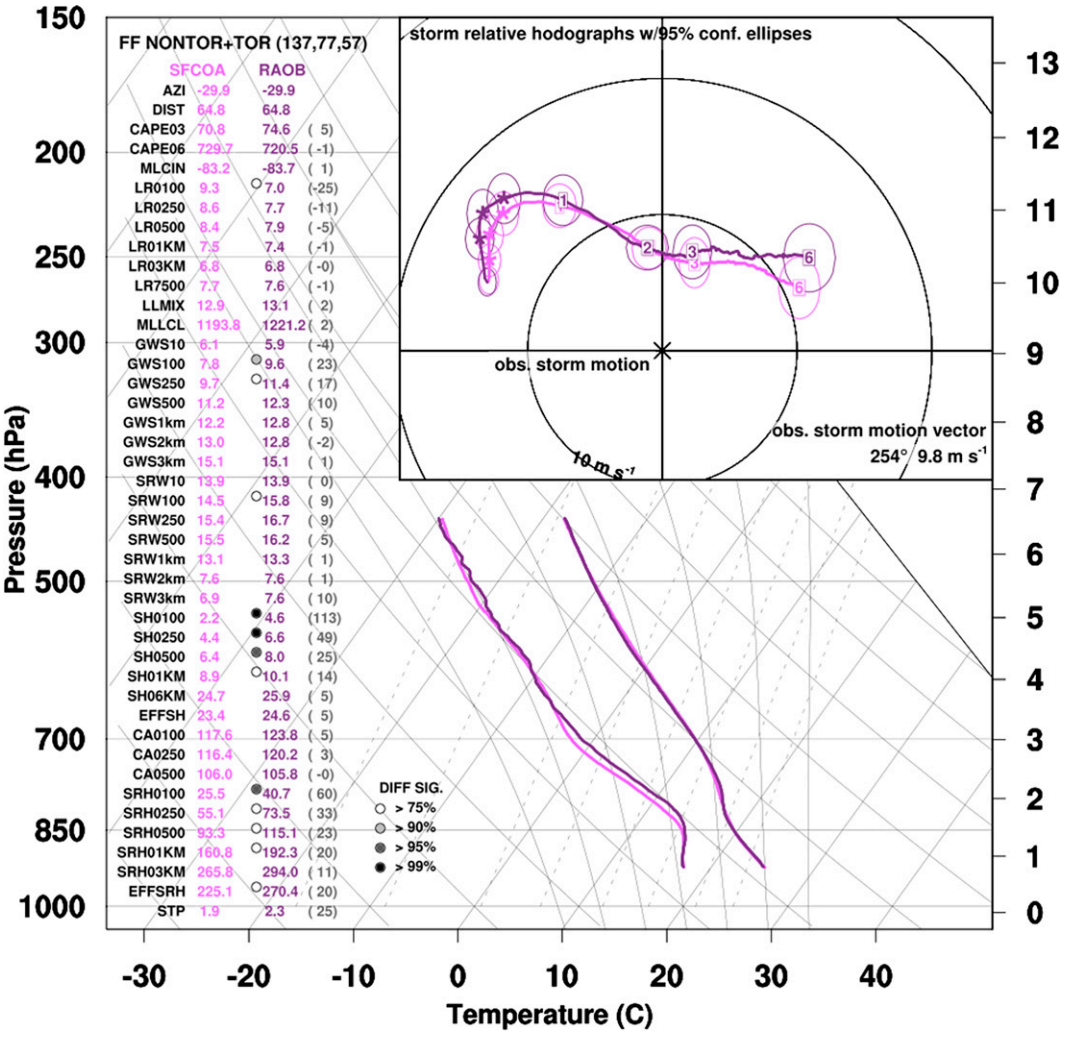

FIG. 4. Mean FF SFCOA (light purple) and raob (dark purple) soundings, hodographs, and severe weather–related variables (means computed from individual soundings before averaging) for the combined NONTOR and TOR subsets. The number of soundings, storms, and unique days in the comparison, respectively, are shown in parentheses in the top left. Statistical significance in the differences of the means is indicated by dots next to the values for the raob subset and are shaded according to significance as shown. Numbers in gray in parentheses indicate the percent change of the mean value for the raob subset from the SFCOA subset. On the hodographs, asterisks are plotted at 100, 250, and 500 m AGL, with height in kilometers AGL up to 6 km indicated otherwise. Ellipses enclose the 95% confidence on the mean wind components. Wind components are remapped to coordinates with the observed storm motion at the origin prior to averaging with the mean ground-relative observed storm motion indicated on the bottom right of the hodograph. Range rings are every 10 m s^{-1}. A description of the variables listed on the left is given in Table 1.

b. Near-field error profiles

To this point, the near-field soundings have been excluded to minimize the potential influences from the storm on the analysis. However, it is important to explore errors in the near-field environment for two main reasons. First, the wealth of studies described earlier that use the RUC/RAP for climatological studies of supercell environments typically use the closest gridpoint and hour to the severe weather report regardless of distance from the storm (although Coffer et al. 2019 did not include the RUC/RAP profile if the convective parameterization was active at that grid point to reduce storm influences). Second, the near-storm environments likely still can control supercell characteristics, and may in fact be quite important to their evolution. The latter is certainly true when external mesoscale features (e.g., a preexisting boundary; Rasmussen et al. 2000) or other nearby storms modify the environment. But some evidence suggests that near-storm environments that are modified by the storm itself can also influence its behavior (Nowotarski and Markowski 2016; Kerr et al. 2019; Flournoy et al. 2020). The following discussions of

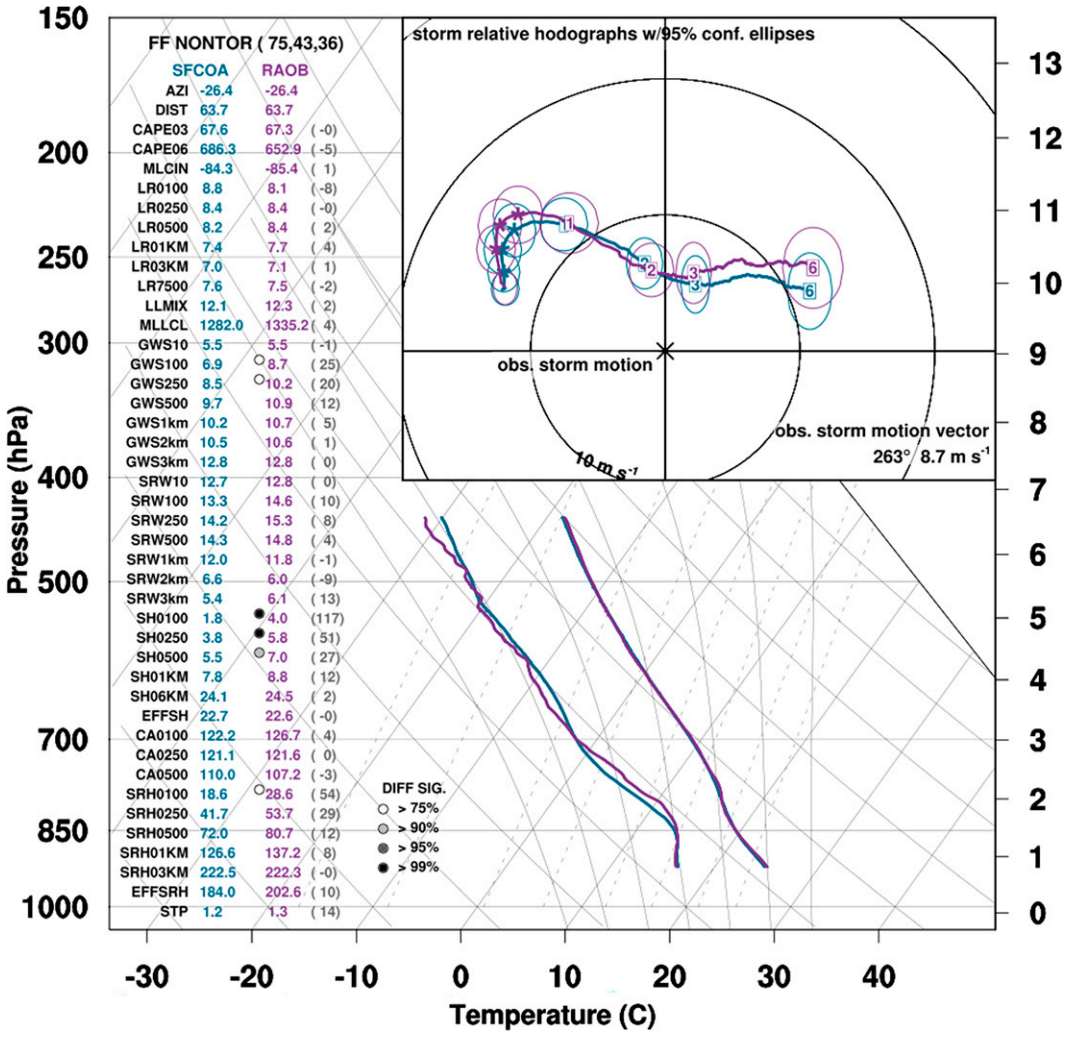

FIG. 5. As in Fig. 4, but for the 75 far-field NONTOR soundings, with the SFCOA in blue and the raobs in purple.

the near-field errors assume that these modified near-field environments are indeed important in determining supercell behavior (but it is recognized that more research is needed to understand the extent to which this is true).

Not surprisingly, the errors in the near field are generally larger than in the far field (Fig. 7). A slight cool bias is now seen in the lowest 500 m and the warm bias in the lower to middle troposphere seen in the far field is exacerbated in the near field. Likewise, the near-field profiles show a larger dry bias than the far-field profiles in the 2.5–5-km layer. On the encouraging side, the nearly unbiased dewpoint profiles below 500 m seen in the far field also are seen in the near field. Collectively, these results show that the near-field SFCOA profiles tend to be too stable in the lower troposphere. This is also shown through significantly larger mean CAPE03 in the near-field raobs than in the near-field SFCOA profiles (Fig. 8).

The SRW error profiles are a strong function of distance from the storm (Figs. 7c,d). A local maximum in the ustm errors is seen near 250 m, with the relatively small MEs in the far-field of 0.5 m s^{-1} increasing to near 2 m s^{-1} in the near field. Above this level, the ustm MEs remain positive up to around 2 km. The MEs in ustm are small above 2 km, but the MAEs are larger in the near field from 2 to 6 km as a result of more variability in the near-field wind profiles. Focusing again near the local maximum near 250 m, the mean vstm errors increase in magnitude from about -2 m s^{-1} in the far field to about -3.5 m s^{-1} in the near field and remain negative, and significantly different at the 95% level from the far-field profiles, up to 6 km (Fig. 7). The dependence of the SRW errors on distance from the storm is underscored in Fig. 9, which shows a clear clustering of the larger mean 0–1-km SRW errors in the sector from $-130°$ to 45° of the storm-relative framework within 40 km of the storm, particularly for the TOR soundings. Figure 9 also shows a shift in the error distribution toward negative values for the TOR soundings, indicating that the larger SRWs are a function of both distance from the storm and tornado production (this is discussed more in section 3c).

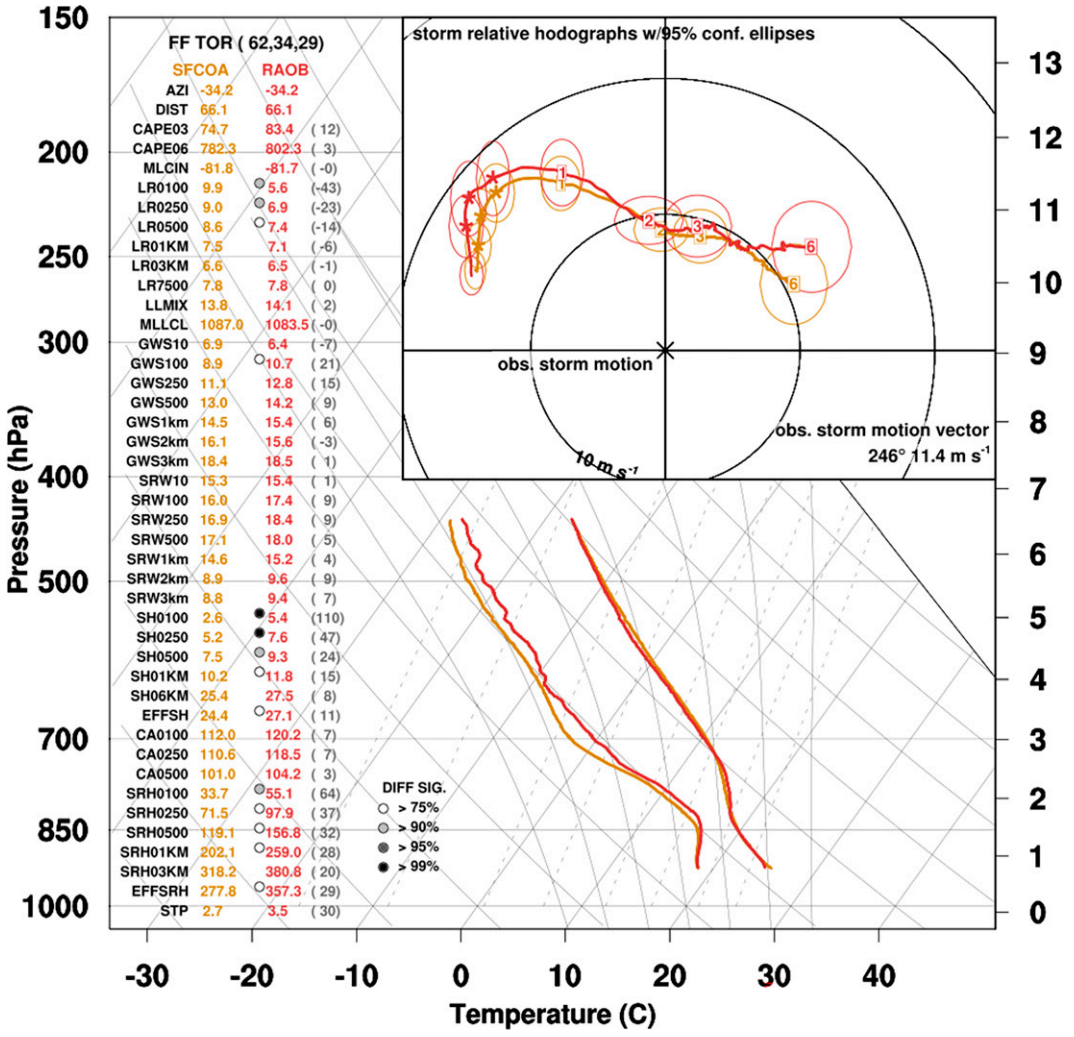

FIG. 6. As in Fig. 4, but for the 62 far-field TOR soundings, with the SFCOA in orange and the raobs in red.

As shown in Fig. 8, the SRW errors result in a substantially larger composite hodograph for the near-field raobs than for the near-field SFCOA. In the near field, in addition to significantly larger near-ground wind shear in the raobs, the near ground SRWs also are significantly larger, and the SRH is now significantly larger in every layer tested (Fig. 8), whereas in the far field, only the SRH0100 was significantly larger for the raobs (Fig. 4). Furthermore, the CAs are now found to be significantly larger, and *farther away* from 90°, in the near-field raobs (Fig. 8), whereas in the far field, there are no significant differences seen for the CAs (Fig. 4).

The errors in both near-field and far-field SRW are maximized at 250 m, and it is likely not coincidental that CP20 found 250 m to be the average height of the hodograph "kink"—a feature often found in supercell environments where the vertical wind profile changes abruptly from predominantly speed shear to directional shear. The height of the kink and magnitude/direction of the winds below the kink relate to potentially important differences in the ratio of near-ground streamwise to crosswise horizontal vorticity ingested into the storm, which has been related to the discrimination of nontornadic and tornadic supercell environments (Esterheld and Giuliano 2008, Coffer and Parker 2018). A CA error below the kink that is counterclockwise and farther from 90°, as seen for the near-field raobs relative to the near-field SFCOA (Fig. 8), likely indicates a larger ratio of streamwise to crosswise horizontal vorticity in the SFCOA than in reality (this is discussed more in section 3c). Figure 2 shows individual examples of the near-ground raob wind shear below the kink being rotated counterclockwise farther from 90° relative to the near-ground SFCOA wind shear.

The mean errors in CAPE03, MLCIN, near-ground lapse rates, SRWs from the surface to 6 km, and the SRH over all layers tested are larger in the near-field TOR soundings than in the near-field NONTOR soundings (Figs. 10 and 11). In contrast, the near-ground wind shear errors and CA errors are actually larger for the near-field NONTOR soundings than the near-field TOR soundings. This shows that the larger

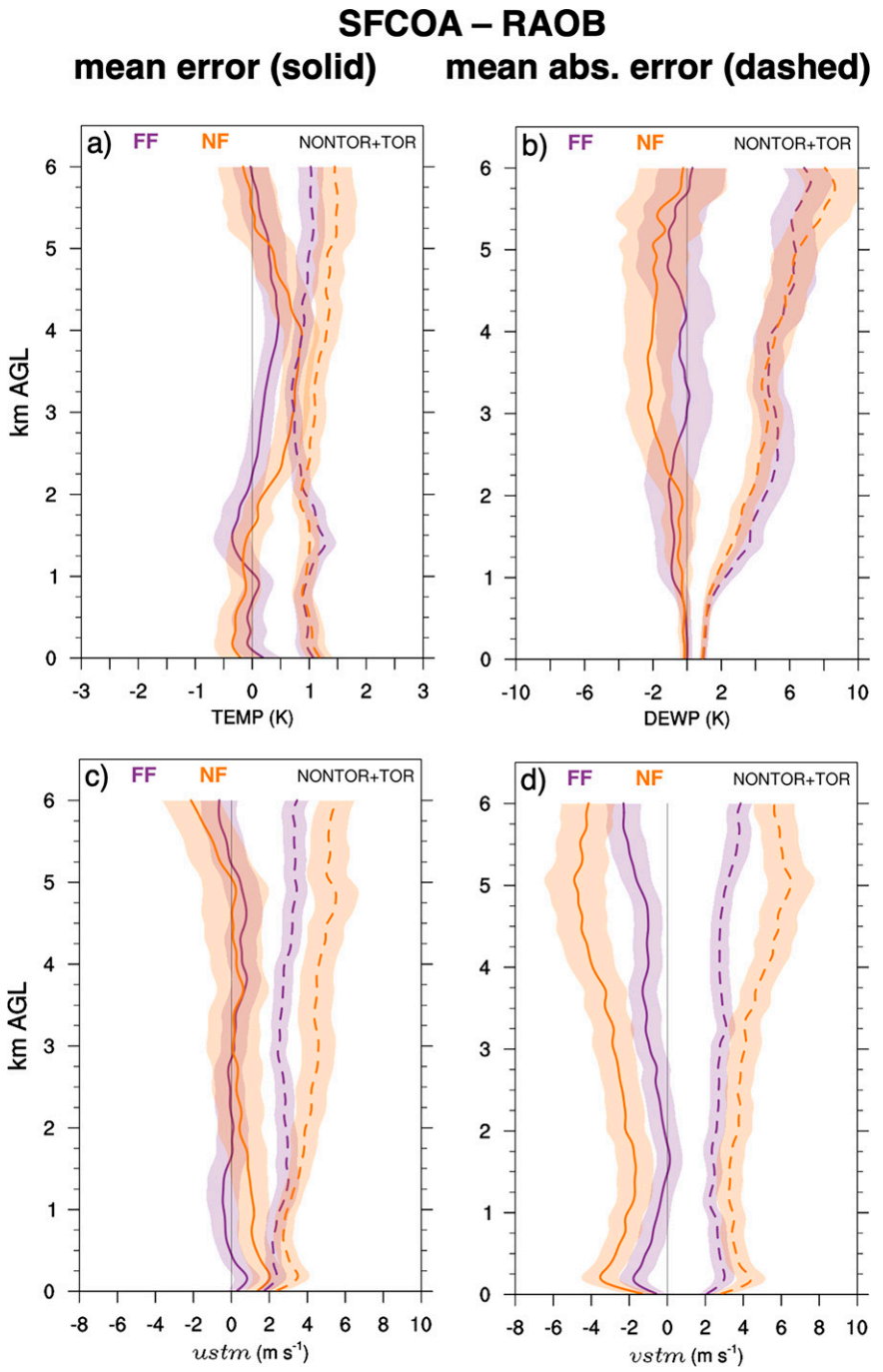

FIG. 7. As in Fig. 3, but the mean error and mean absolute error profiles for the 120 near-field (NF) soundings are added in orange.

SRH errors seen for the near-field TOR soundings are driven primarily by the larger SRW errors. In fact, the composite hodographs for the near-field TOR soundings show little to no overlap in the 95% confidence ellipses at all levels, particularly below 1 km (Fig. 11). Collectively, these errors in SRW, shear, SRH, and CA lead to important differences in diagnostic variables for supercell tornado potential, as examined next.

c. *NONTOR versus TOR composites*

The above analysis showed that errors in many variables are a function of distance to the storm and tornado production. To facilitate an analysis of how interpretations of the discriminatory ability of severe weather–related variables may change when using the SFCOA instead of the raobs, composite soundings are produced that compare the NONTOR and

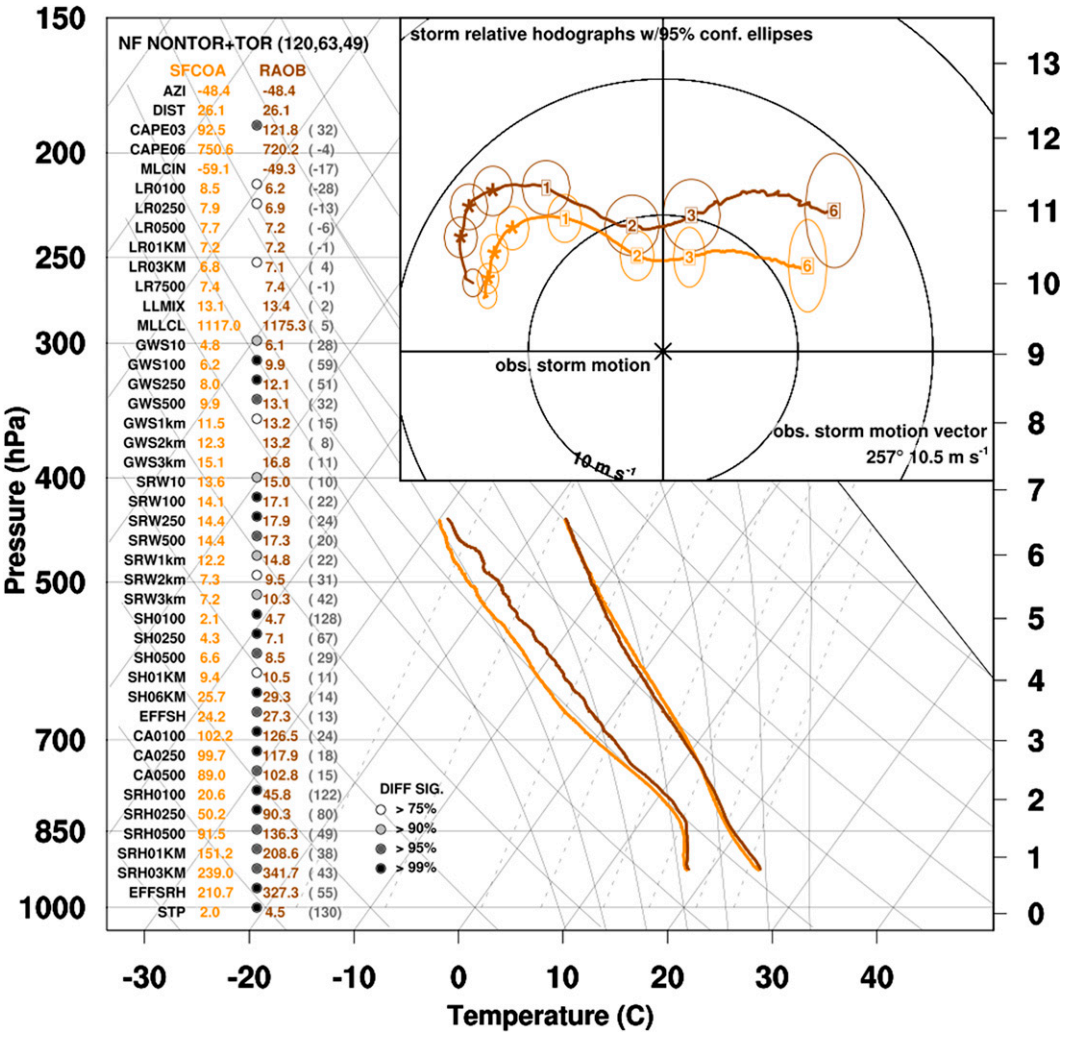

FIG. 8. As in Fig. 4, but for the 120 near-field (NF) soundings, with the SFCOA in orange and the raobs in brown.

TOR subsets for the combined near-field and far-field profiles (Figs. 12 and 13; these composites now compare the NONTOR and TOR subsets on the same skew T–log$p$ hodograph instead of the SFCOA and raob subsets).

For most variables, the sign of the mean differences in the variables between the NONTOR and TOR raob subsets does not change when switching from the raobs to SFCOA. For example, the mean MLLCL is still smaller for the TOR soundings and the mean 0–1-km SRH is still larger for the TOR soundings than for the NONTOR soundings regardless of the dataset used. One exception is seen for the near-ground lapse rates (Figs. 12 and 13), as discussed previously.

However, there are several notable changes in the *magnitude* of the differences in the mean variables between the NONTOR and TOR soundings when switching from the raobs to the SFCOA profiles. For the thermodynamics, the mean CAPE03 in the raobs is 26% larger for the TOR soundings than the NONTOR soundings (and statistically significant at the 90% level), but is only 10% larger in the SFCOA soundings. This suggests that the use of SFCOA might underrepresent the ability of CAPE03 to discriminate between nontornadic and tornadic supercells. As seen earlier, the near-field soundings are contributing much more to the CAPE03 errors than the far-field soundings, and the TOR soundings contribute more than the NONTOR soundings.

The more substantial changes in interpretation when switching to the SFCOA soundings are seen for the kinematic variables. The composite hodographs show less separation in the NONTOR and TOR composite hodographs below 2 km when using the SFCOA (cf. Figs. 12 and 13). This can also be seen in the mean SRW values on Figs. 12 and 13: the mean SRWs below 2 km are significantly larger for the TOR soundings than the NONTOR soundings when using the raobs (Fig. 12) but are less so when using the SFCOA (Fig. 13).

Relating this result of substantially larger low-level SRWs for the TOR soundings to past work, Thompson et al. (2003) and Markowski et al. (2003) show no significant differences in SRW below 2 km between tornadic and nontornadic supercell

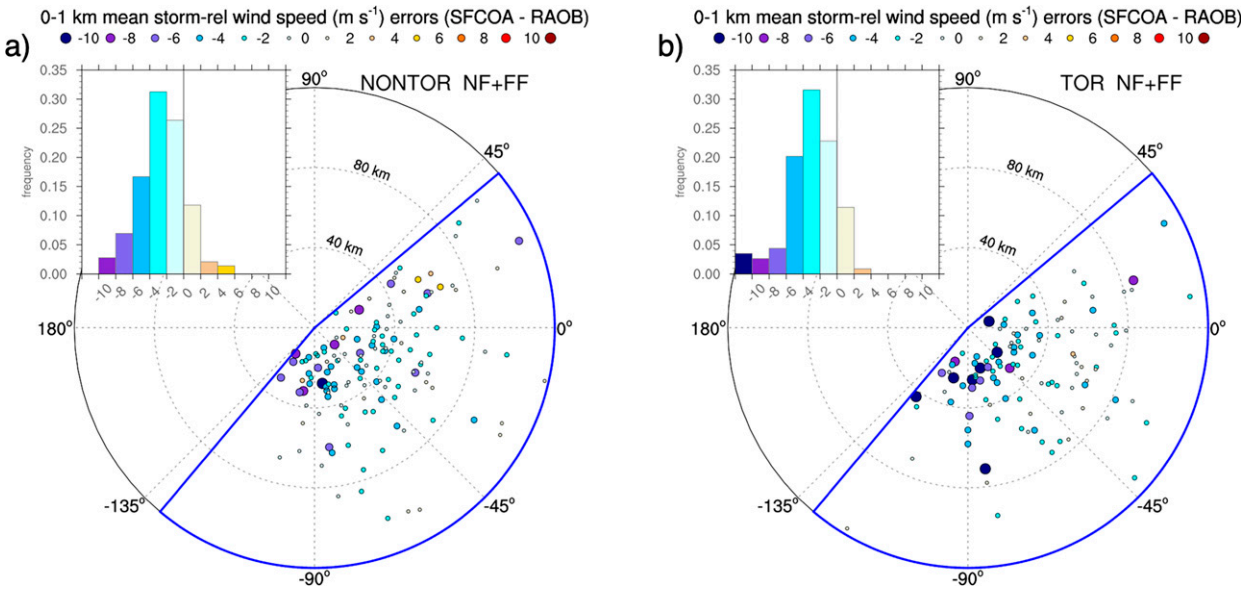

FIG. 9. SFCOA errors in the mean 0–1-km SRW (m s^{-1}) for (a) 143 NONTOR soundings and (b) 114 TOR soundings. The errors are plotted in their storm-relative location (the storm at the origin with motion along the x axis). The magnitude of the errors scale with the size of the dots and are color shaded according to the legends at the top of each panel (the dots represent errors between the values shown in the legend). The inset in each panel displays a binned distribution of the errors, with the same color shading as is used for the dots (the first and last bins include all values less than or greater than the second-to-last bin value). Range rings are every 40 km. The blue polygon outlines the area used to define a proximity sounding for this study (except for within 10 km of the storm).

environments using RUC/RAP soundings within 40 km of the storm. Although the RUC version used in Thompson et al. (2003) and Markowski et al. (2003) is over 20 years old at the time of this writing, those results may still be relevant if resolution is the primary cause since that version used only one less vertical level than recent versions (50 vs 51; Benjamin et al. 2016). This shows that *the SRW errors in the near-field environment (caused by either preexisting features or by the storm itself) likely prevent RUC/RAP-based analyses from identifying low-level SRWs as an important variable that discriminates nontornadic and tornadic supercell environments in past studies*. This could also be impacting the results of Nowotarski and Jensen (2013) who find SRW to be more skillful in nonsupercell regimes than supercell regimes, as well as the results of Coffer et al. (2019), who find little to no difference in SRW between significantly tornadic (F/EF2+) and nontornadic supercells using the SFCOA [see Fig. 3 in Coffer et al. (2020) for these profiles].

The larger SRW errors for the TOR soundings than the NONTOR soundings lead to changes in interpretation of the relative importance of shallow versus deep-layer SRH variables in discriminating nontornadic and tornadic supercells. For example, when using the raobs, the mean EFFSRH is 74% larger for the TOR soundings than the NONTOR soundings (389 m^2 s^{-2} vs 224 m^2 s^{-2}; Fig. 12) but is only 40% larger when using the SFCOA (260 m^2 s^{-2} vs 185 m^2 s^{-2}; Fig. 12). However, when using the raobs, the mean SRH0500 is 54% larger for the TOR soundings than the NONTOR soundings (155 m^2 s^{-2} vs 101 m^2 s^{-2}; Fig. 12) and is 41% larger when using the SFCOA (110 m^2 s^{-2} vs 78 m^2 s^{-2}; Fig. 12). In other words, the separation in mean SRH between the TOR and NONTOR soundings is similar for SRH0500 and EFFSRH when using the SFCOA, but the separation in mean SRH between the TOR and NONTOR soundings is larger for EFFSRH than SRH0500 when using the raobs. This suggests that *the use of the SFCOA on this dataset would deemphasize the importance of EFFSRH relative to the near-ground SRH in comparison with use of the raobs*. To show that the mean of the variables is sufficient to make this determination, Fig. 14 shows the distribution of the SRH0500 and EFFSRH errors for the NONTOR and TOR soundings, along with their individual storm-relative locations. The distributions in errors shift toward negative values from the NONTOR to the TOR soundings more so for the EFFSRH than for the SRH0500. Figure 14 also serves to show that, while SRH errors tend to be larger in the near field, substantial SRH0500 and EFFSRH errors still do occur in the far field, and conversely, that a location in the near field does not necessarily mean that the SRH errors will be large. Furthermore, SRH0500 and EFFSRH are not as large a function of distance from the storm as the mean 0–1-km SRW (cf. Figs. 9 and 14).

The above comparison of SRH0500 and EFFSRH has potentially important implications when interpreting the results of Coffer et al. (2019). They show that the incorporation of SRH0500 into the significant tornado parameter (STP) (Thompson et al. 2012) increases skill over the traditional EFFSRH-based STP when discriminating significantly tornadic and nontornadic supercells. If the results found here for EFFSRH translate broadly, the true skill of the EFFSRH-based STP could be underestimated in that study because of

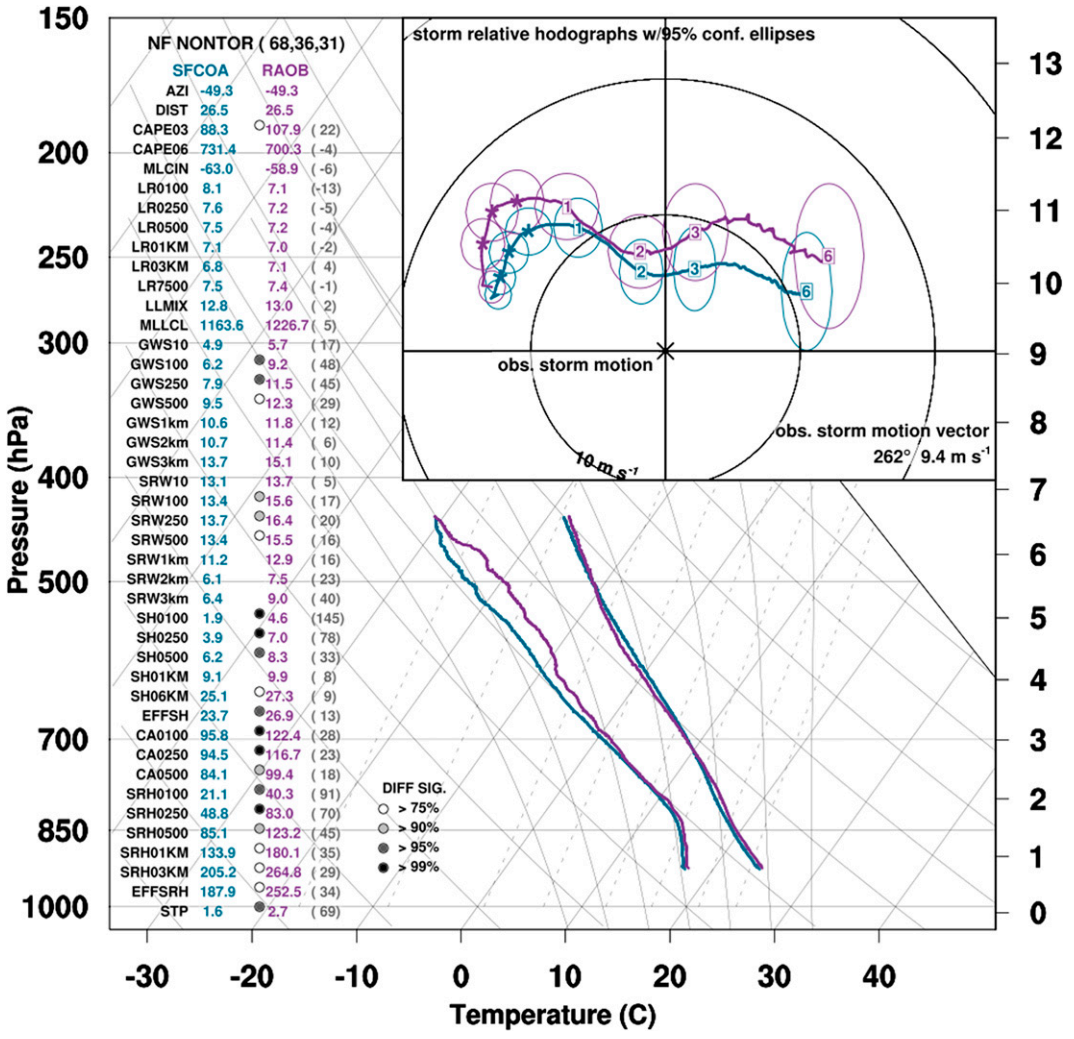

FIG. 10. As in Fig. 4, but for the 68 NF NONTOR soundings, with the SFCOA in blue and the raobs in purple.

the use of the SFCOA soundings. However, the general nature of this assertion will need to await a study that incorporates the much broader geographical and seasonal diversity in cases included in Coffer et al. (2019). This is because Coffer et al. (2019) find the forecast skill of SRH500 to decrease relative to EFFSRH when the dataset is restricted to April, May, and June cases in the southern Plains. Essentially, the forecast skill between SRH500 and EFFSRH is roughly the same for a similar regional and seasonal time frame as the soundings in this study and in CP20. This does not explain the finding here of larger separation between nontornadic and tornadic soundings for deeper layers of SRH when using the ROABs versus the SFCOA, but this does suggest that the best forecast potential of using near-ground SRH may not be covered in this study due to a sampling bias of using only storms from field projects in the central United States.

Returning to what can be gleaned from this dataset, SFCOA EFFSRH shows larger decreases in separation between the NONTOR and TOR soundings than the SFCOA SRH0500 partly because it is integrated over deep layers; in these layers, differences in SFCOA SRWs between the NONTOR and TOR soundings are consistently smaller. Evidence that the SRW errors and not wind shear errors are primarily driving the increase in SRH differences when using the raobs comes from separations in mean near-ground wind shear between the NONTOR and TOR soundings that are actually *larger* when using the SFCOA than when using the raobs (cf. SH0100, SH0250, and SH0500 on Figs. 12 and 13). Conversely, the separations in mean SRW between the NONTOR and TOR soundings are larger when using the raobs for all levels $\leq$ 2 km. In other words, the SFCOA is overemphasizing the differences in shear between the NONTOR and TOR subsets and underemphasizing the differences in deeper-layer SRH (and SRW) between the NONTOR and TOR subsets.

Another interesting finding when comparing Figs. 12 and 13 is that the separation in mean CAs between the NONTOR and TOR soundings remain very small regardless of the dataset

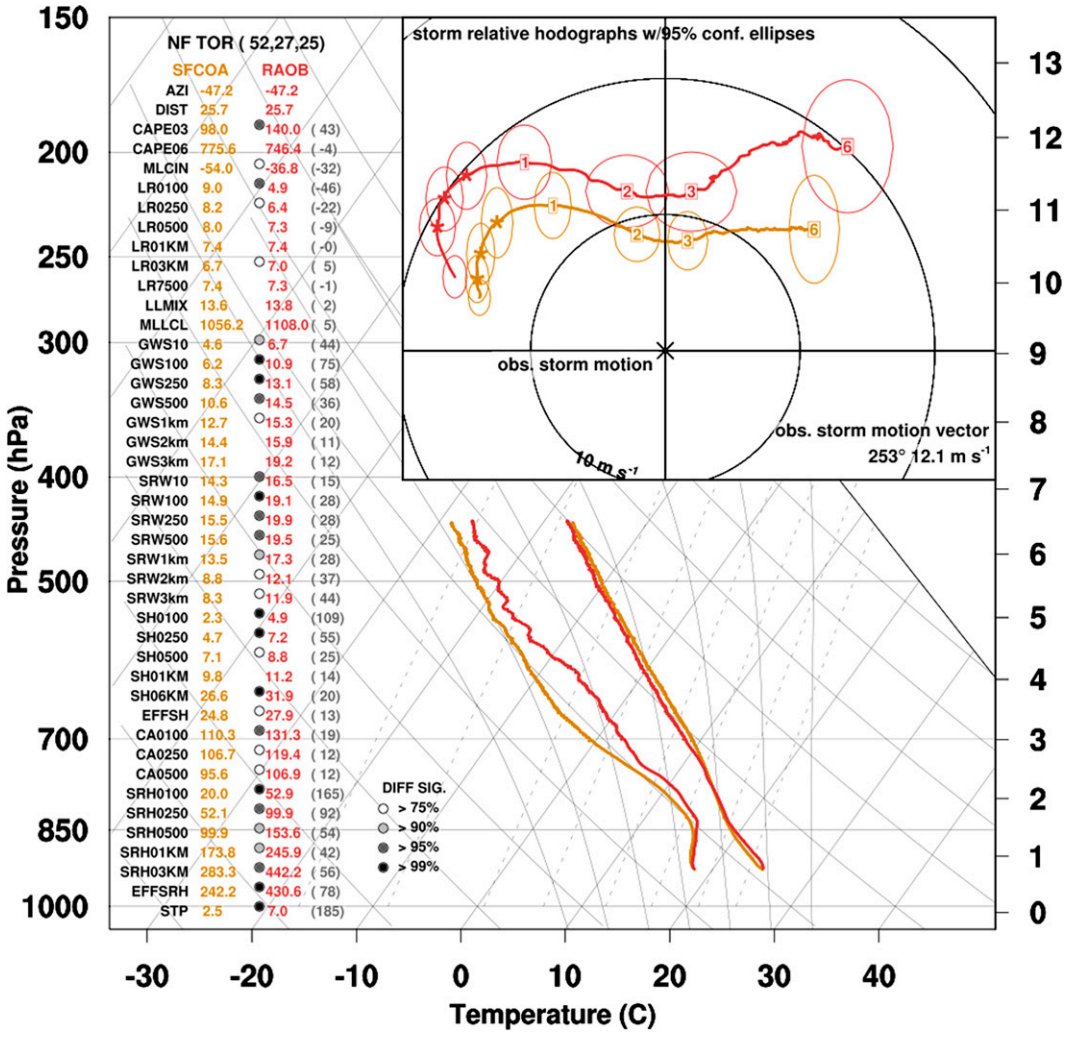

FIG. 11. As in Fig. 4, but for the 52 NF TOR soundings, with the SFCOA in orange and the raobs in red.

used. This shows that the use of the SFCOA does not change the interpretation of the importance of the CAs in discriminating between the NONTOR and TOR soundings; both Coffer et al. (2019) and CP20 find negligible differences in mean CAs between TOR and NONTOR subsets (but fewer CAs closer to 180° or 0° for the TOR soundings), and the use of SFCOA here does not change that interpretation. However, as shown earlier in Fig. 8, the mean CAs are 5°–15° larger overall when using the raobs instead of the SFCOA profiles, and these CAs are *farther* from 90°. This would often give an impression that the CAs were closer to 90° in the SFCOA profiles than in reality. A CA of 90° likely indicates an environment with a high ratio of streamwise-to-crosswise horizontal vorticity in the lowest 500 m (it is only an approximation of the streamwise horizontal vorticity), and so caution is encouraged when using RUC/RAP-based analyses for supporting arguments on the importance of a high ratio of near-ground streamwise to crosswise horizontal vorticity relative to other factors.

4. Summary and conclusions

Numerous climatological studies aimed at defining the environment of convective storms use the SFCOA, or other RUC/RAP-based datasets, produced on 25-hPa levels as a proxy for observed soundings. However, errors in doing so are not well understood. This study presents a comparison of high-resolution field-project rawinsondes collected near supercells to profiles extracted from the SFCOA to quantify these errors and understand better the reasons for discrepancies in recent studies of supercell environments. Observed soundings obtained close to the supercells (within 10–120 km from the storm) are included in this analysis and provide a means to understand errors in the SFCOA in near-supercell environments.

a. Summary of main results

Errors in kinematic variables are generally more substantial than errors in thermodynamic variables. For the latter, temperature errors are relatively small, but a small low-level cool bias

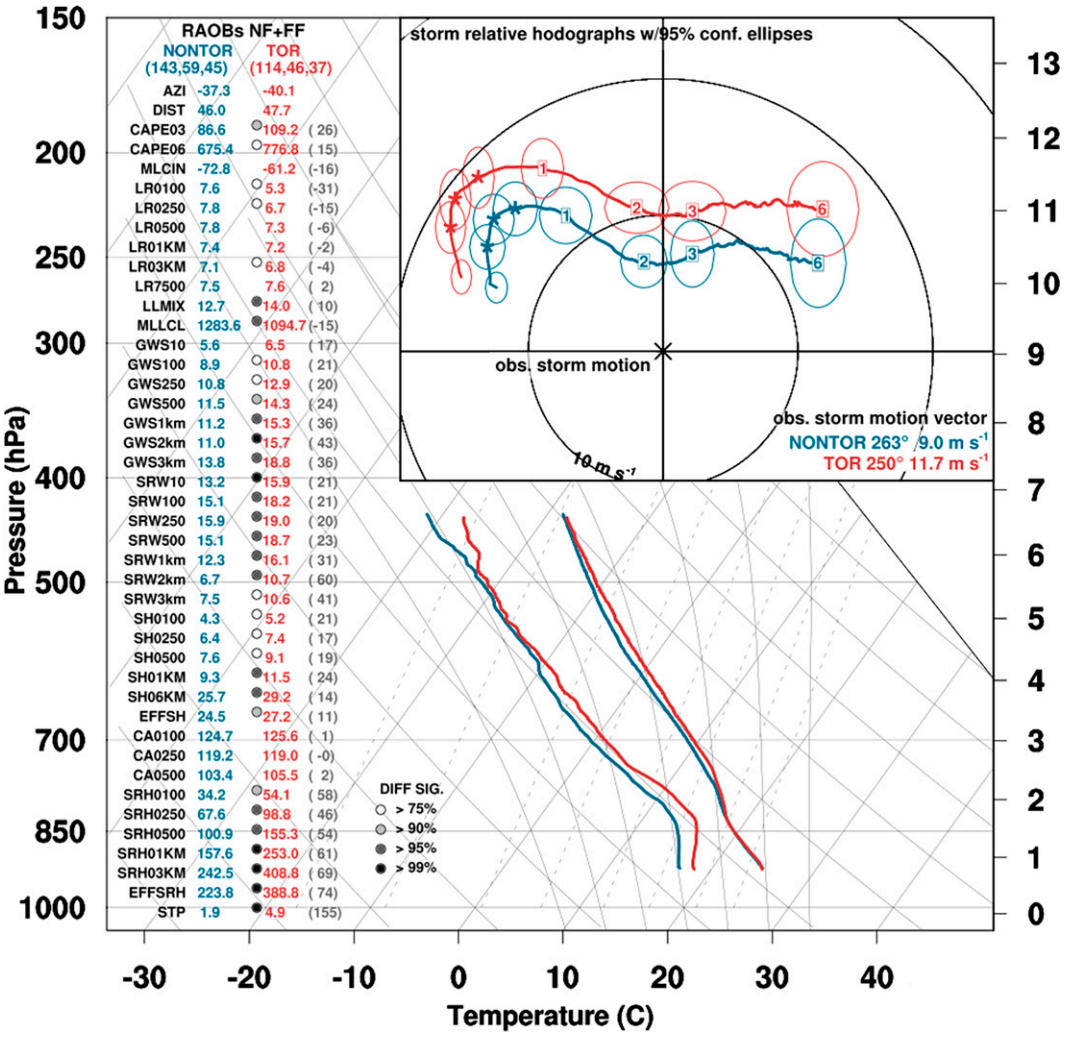

FIG. 12. As in Fig. 4, but for a comparison of the 143 NONTOR raobs and 114 TOR raobs for the combined NF and FF subsets.

and a modest warm bias in the few kilometers above the boundary layer, most prevalent closer to the storm and for the TOR soundings, leads to 0–3-km CAPE that is too small in the near field. Somewhat surprisingly, the dewpoints below 500 m are nearly unbiased, but do show a dry bias above the boundary layer, particularly for the near-field and TOR soundings. The TOR soundings show larger errors in the near-ground lapse rates than the NONTOR soundings, relating to shallow stable layers seen in the observed soundings, mostly in the TOR subset.

A primary result is that the SFCOA underestimates the low-level storm-relative winds and wind shear. The near-ground (≤500 m) wind shear is underestimated similarly in both near-field (10–40 km) and far-field (40–120 km) environments and in TOR and NONTOR soundings. The near-ground storm-relative winds, however, are underestimated the most in the near field and in the TOR soundings, although it should be noted that a slow storm-relative wind bias also is seen in the far-field and NONTOR soundings, just not as large as that seen in the near-field and TOR soundings. *Slow SRW errors are therefore a likely contributor to the lack of differences in storm-relative winds between nontornadic and tornadic supercell environments in past studies that use RUC/RAP-based analyses.*

Storm-relative wind errors that increase with decreasing distance to the storm is likely indicative of accelerations induced by perturbation low pressure associated with the storm itself, although enhancements from preexisting mesoscale perturbations or other nearby storms could also be playing a role. The larger errors in near-ground storm-relative winds for the TOR soundings likely relates to the tornadic mesocyclones that were shown in CP20 to be more impactful to their surrounding environment than the nontornadic mesocyclones. The SFCOA analyses do not depict this larger influence from the tornadic mesocyclones.

The mean critical angles (angles between the near-ground shear vector and the storm motion) are 5°–15° larger, and

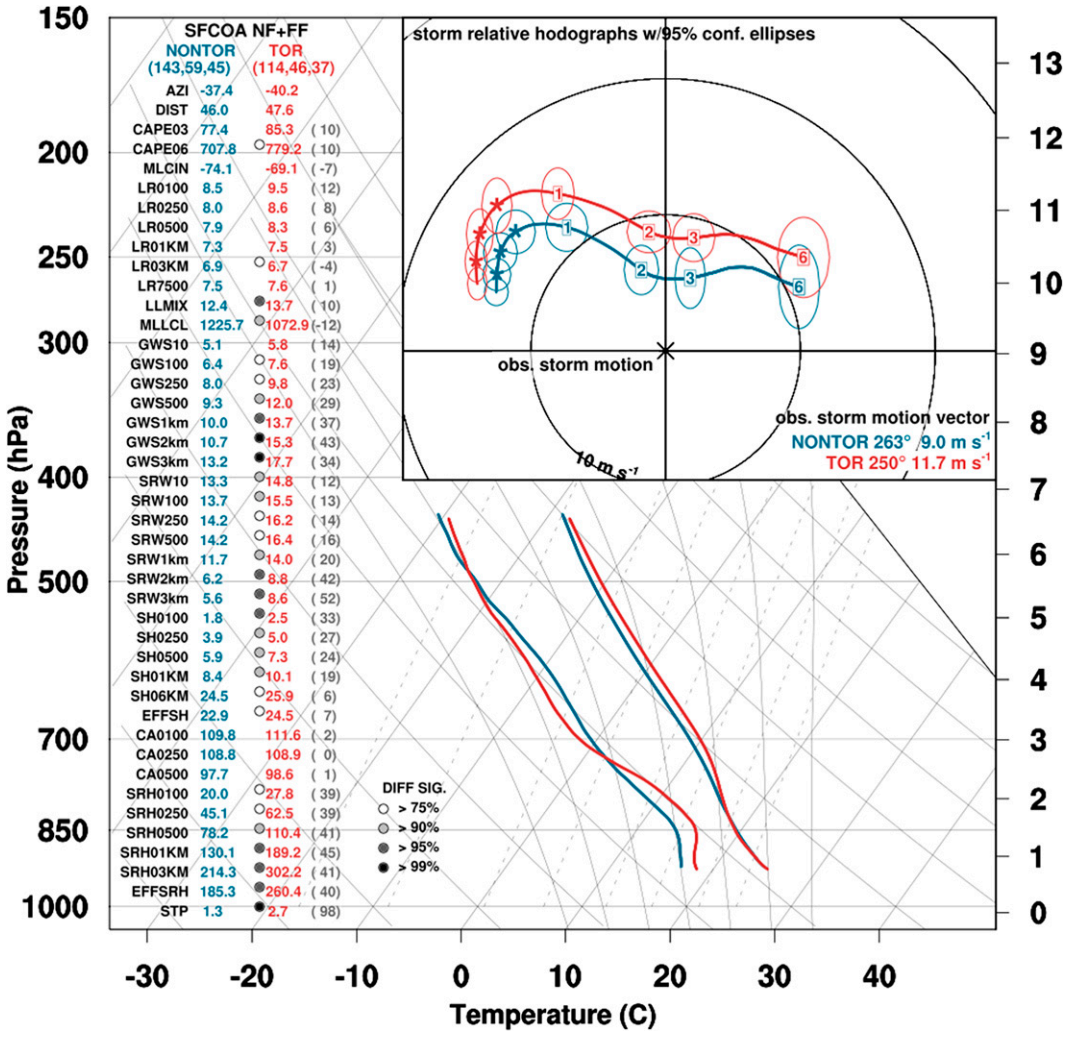

FIG. 13. As in Fig. 4, but for a comparison of the 143 NONTOR SFCOA soundings and 114 TOR SFCOA soundings for the combined NF and FF subsets.

farther from 90°, in the observed soundings than in the SFCOA profiles. These errors are not a strong function of tornado production but are larger in the near field. This indicates that the near-field environment, on average, likely does not have as high a ratio of streamwise to crosswise horizontal vorticity as suggested by the SFCOA profiles, although an encouraging sign is that the use of the SFCOA profiles does not change the relative difference in CAs between the NONTOR and TOR environments, only the values of the CA overall.

However, the separation in mean variables between the NONTOR and TOR soundings is larger for the effective SRH than for the 0–500-m SRH when using the observed soundings instead of the SFCOA profiles. Unlike for SRW, the CA errors and wind shear errors are not strong functions of the dataset used. Therefore, the increased separation in SRH with deeper layers between the NONTOR and TOR soundings when using the observed soundings instead of the SFCOA profiles is driven primarily by the increased separation in mean SRW between the NONTOR and TOR soundings when using the observed soundings instead of the SFCOA profiles.

The above suggests the use of the SFCOA or RUC/RAP-based analyses could underemphasize the true importance of the effective SRH relative to shallower SRH in discriminating nontornadic from tornadic supercells. This does not mean that near-ground SRH is not a good discriminator of tornadic and nontornadic supercells in the plains—in fact our results show significantly larger near-ground SRH in tornadic environments (Fig. 12). Our results also show, however, a larger percentage increase in mean deeper-layer SRH from the nontornadic to tornadic soundings than for mean near-ground SRH (Fig. 12), suggesting that deeper-layer SRH may have just as much, if not more, discriminatory power in this dataset than near-ground SRH. CP20 hypothesized for why this might be the case, including the enhancement of SRH aloft as storm motion deviates to the right (see their Fig. 11) and stronger SRWs aloft that help to distribute hydrometeors away from

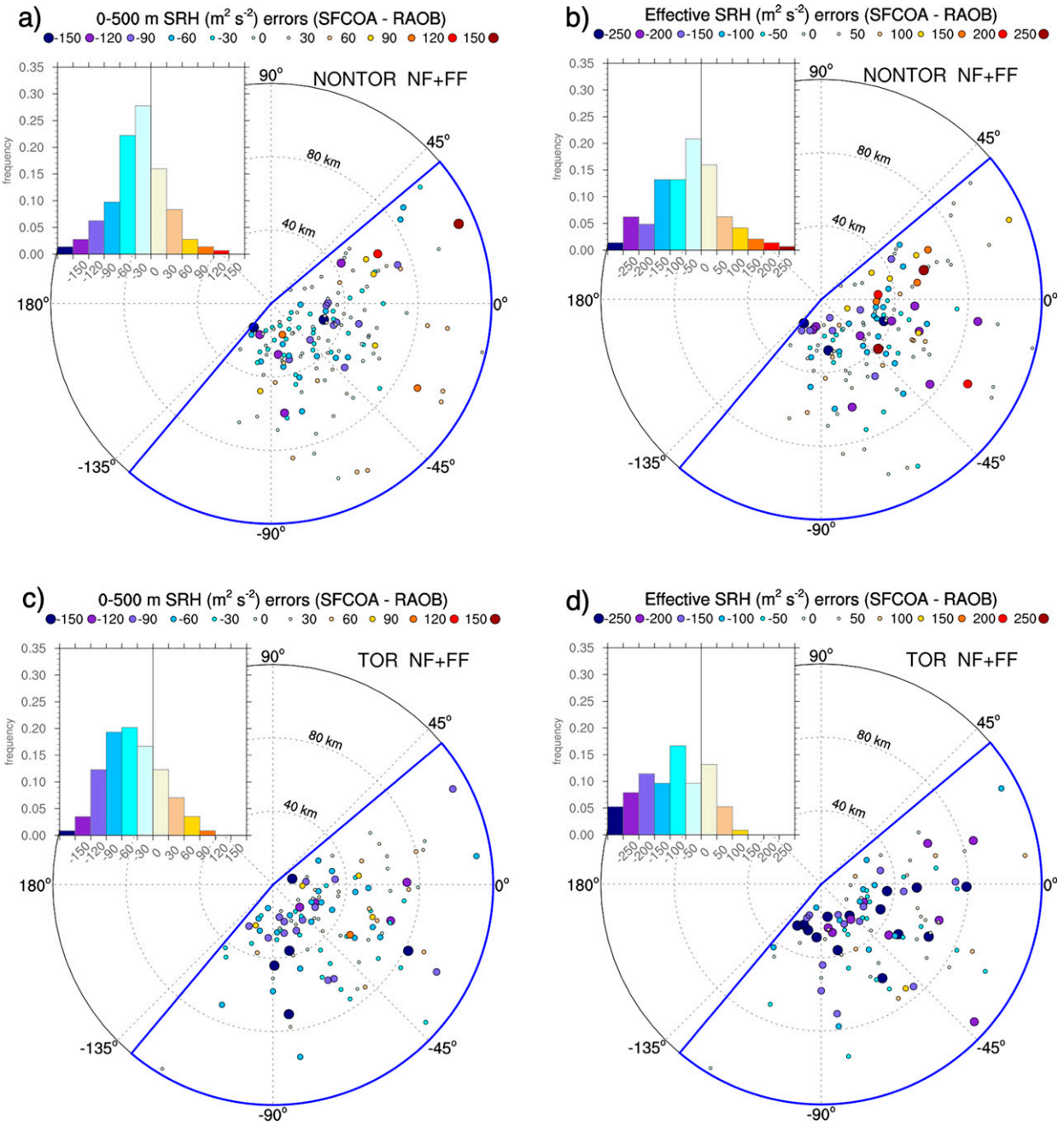

FIG. 14. As in Fig. 9, but for errors in (left) SRH0500 and (right) EFFSRH ($m^2 s^{-2}$) for the (a),(b) 143 NONTOR soundings and (c),(d) 114 TOR soundings.

the updraft that hinders excessive cold-pool development. Therefore, EFFSRH may be incorporating favorable tornadic processes that happen both close to the ground (e.g., those shown in Coffer and Parker 2017, 2018) along with those that occur farther aloft.

b. Final discussion and synthesis

By design, the RUC-RAP-based analyses represent the storm environment unmodified by convection (with the small caveat of latent heating adjustments in the digital filter initialization). It is important to note that the result shown here of increasing errors with decreasing distance to the storm for many variables should not be considered a flaw of the SFCOA per se, but rather something that should be considered when constructing and interpreting storm–environment relationships using RUC/RAP-based analyses. This study shows that the 40-km postprocessed SFCOA grids with 25-hPa levels often does not depict modifications to the

environment that can occur close to the storm. These modifications are likely induced by the storm itself to a significant degree, but they also could be indicative of small mesoscale features of the environment (e.g., outflow boundaries or enhanced inflow induced from other nearby storms).

We can only speculate on the exact causes for the underrepresentation of near-ground wind speeds and errors in other near-ground variables, like lapse rates. The vast difference in vertical resolution between the raobs and the native RUC/RAP levels is likely a primary contributor, but the representation of subgrid turbulent mixing in the RUC/RAP model[8] could also play a substantial role. Even with very high vertical resolution, deficiencies in depicting turbulent mixing and surface exchanges can result in substantial near-ground wind speed errors, especially in strong synoptic forcing regimes (e.g., Cohen et al. 2017) and as the atmosphere transitions from afternoon to evening boundary layers (e.g., Mirocha et al. 2016; Smith et al. 2018). However, the converse also is true: a perfect turbulent mixing scheme in a model with only 5–6 levels below 500 m as in the RUC/RAP native levels still may not resolve the abrupt increase in wind speeds above the surface layer in the few hundred meters above the ground that often characterizes supercell inflow.

Note that, while evidence presented here suggests the use of RUC/RAP-based analyses can mislead on the importance of near-ground and near-field severe weather–related variables, a contribution from sampling bias cannot be ruled out. This study employs the largest sample of high-resolution observed soundings to be used in supercell environment studies to the authors' knowledge, but the sample sizes still pale in comparison with those that use the SFCOA; for example, Coffer et al. (2019) include over 20 000 SFCOA profiles in their study from all parts of the United States, whereas this study is limited to a few hundred soundings from mostly springtime events in the southern and central plains (Fig. 1) when/where supercell-related field projects have historically taken place. Even when using only the SFCOA, the sample used here identifies differences in SRW between the NONTOR and TOR soundings (albeit not with high statistical significance; Fig. 13) that are not seen in other supercell environment studies that use RUC/RAP-based analyses. It remains possible that the signal of stronger SRWs in tornadic supercell environments is limited to supercells in the somewhat narrow region/time of year in this study. A logical next step is to explore errors in RUC/RAP-based profiles in supercell environments in other parts of the United States and times of the year.

We also emphasize that, even without resolving the near-storm differences in the environment, the SFCOA (and the RUC/RAP in general), in practice, has proven to be a useful tool in severe weather forecasting (Thompson et al. 2007; Hart and Cohen 2016; Coffer et al. 2019) indicating that it is capable of resolving important environmental differences that discriminate tornadic from nontornadic supercells. Even with errors in the underlying analysis, forecaster calibration to the differences in tornadic and nontornadic environments in the analyses is still useful. However, this study takes the viewpoint that the lack of resolving near-storm environments in the analysis could be limiting our forecast skill and assessment of tornado potential. This viewpoint assumes that the modifications in the near-storm environment are not simply passive to the storm, but can feed back to changes in storm evolution, as suggested in Nowotarski and Markowski (2016), Kerr et al. (2019), and Flournoy et al. (2020). Admittedly, it is not clear how much of this is true; i.e., when the "storm" ends and the dependence on the environment begins. This has long been a topic in storm–environment studies—see Weisman et al. (1998)—but has not received much attention in the past few decades. It is likely that the real atmosphere falls between the extremes of the fate of the storm being completely predetermined by the preconvective and background environments, to being completely susceptible to evolutionary changes brought out by the storm-induced modifications; but where the atmosphere tends to fall in this range of possibilities is still uncertain. Furthermore, it can be hypothesized that local changes to the storm environment are at least partly responsible for the typical large variability in storm outcomes in seemingly similar large-scale environments (e.g., Coffer and Parker 2017; Markowski 2020). The lack of accuracy in the SFCOA near-field analyses could then be a reason why skill extracted from mesoscale model analysis storm/environment relationships is ultimately limited.

Note that this study did not examine the use of convection-allowing models (CAMs; e.g., from the HRRR) to examine environmental relationships, which have the potential to better resolve boundary layer evolution (e.g., Evans et al. 2018; Fovell and Gallagher 2020) and capture local environment changes brought about by convection. For example, Potvin et al. (2020) show that supercells predicted by the NSSL Warn-on-Forecast System (WoFS; Lawson et al. 2018) often show local enhancements to SRH in their near inflow in a qualitatively accurate sense, but the realism of these modifications is not clear. The WoFS also may have the ability to assimilate small mesoscale features into the initial condition that may be responsible for enhanced environments near the storm. Work is ongoing at NSSL to quantify the accuracy of these local environment changes in WoFS and in similar CAMs. This work is important since by 2024, EMC plans to implement the CAM-based Real-Time Mesoscale Analysis (3D-RTMA) system, a tool that is expected to supplant the SFCOA for diagnosing the mesoscale environment for severe weather applications.

Furthermore, this study did not examine the ERA5 reanalyses that have many more gridpoints near the ground than the RUC/RAP analyses (e.g., Coffer et al. 2020), although it is not clear if the effective resolution of the ERA5 profiles would offer significant improvement since Taszarek et al. (2021) finds the ERA5 to underestimate low-level wind shear, particularly for the larger values that often occur in supercell inflow. Finally, because the focus here is on the 25-hPa dataset since this is used widely in both climatological studies of supercell environments and in operational forecasting, the accuracy of

[8] The RUC/RAP used variations of the the Mellor–Yamada–Janjić (Janjić 2001) and Mellor–Yamada–Nakinishi–Nino (Nakanishi and Niino 2009) turbluence-mixing schemes over the period of this study.

the analyses extracted from RAP/RUC native hybrid-sigma levels was not examined thoroughly. A comparison of the 2019 13-km RAP native-level data to the 40-km SFCOA data showed no substantial or clear, systematic differences, but there was some indication of a modest improvement in the analyses in the lowest 500 m in some cases (not shown). Therefore, a comprehensive comparison of the native-level data with the SFCOA, or more generally the impacts of vertical resolution on analyses of storm environments, is encouraged.

Ultimately, we hypothesize that assimilation systems may require observations at comparable resolution to the underlying models to accurately capture the potentially important local modifications to the environment in their analyses. For example, dual polarimetric variables in radar observations can estimate local changes in SRW and SRH (Kumjian and Ryzhkov 2012; Wilson and Van Den Broeke 2021). A promising way to observe the winds at high vertical resolution near storms involves the use of Doppler wind lidars (e.g., Coniglio et al. 2019; Markowski et al. 2019; Wagner et al. 2019), and methods of obtaining humidity measurements at resolutions comparable to radiosondes using ground-based remote sensing appear promising (Weckwerth et al. 2016). Research is ongoing at NSSL to better quantify the value that these experimental observing systems can add to assessments of the near-storm environment to aid in situational awareness for operational forecasters and in improving the initial conditions for convection-allowing assimilation and forecast systems. However, it should be emphasized that, until we are able to accurately sample or analyze the near-storm environment routinely, useful relationships uncovered in studies that use the SFCOA and similar analysis systems should continue to be relevant as forecast guidance in the near future, despite the deficiencies presented in this paper.

Acknowledgments. We thank Brice Coffer and two anonymous reviewers for helpful and constructive comments and suggestions that improved this paper. We thank Matthew Flournoy, Erik Rasmussen, Bryan Smith, Rich Thompson, and Israel Jirak for early reviews of this work and their helpful comments. The partnership between SPC and NSSL, which led to the first author—an NSSL researcher—working operational shifts at SPC, has further cultivated the relationship between research and operations and provided motivation for this work. The authors greatly thank NSSL and SPC leadership for supporting this collaboration. SFCOA data are maintained at the SPC by Andy Dean. Radiosonde data used were obtained with support from multiple NOAA discretionary funding and National Science Foundation awards, including VORTEX2 (AGS–1748715), MPEX (AGS-1230114), PECAN (AGS-1359726), and TORUS (AGS-1824811). Figures were made using the NCAR command language (NCL), version 6.6.1.

Data availability statement. Most radiosonde data used during this study are openly available from the NCAR Earth Observing Laboratory Data Archive (https://data.eol.ucar.edu/). These data were reanalyzed by the first author. All of the data analyzed for this study and further information about data processing are available upon request from the National Severe Storms Laboratory through the first author (michael.coniglio@noaa.gov).

REFERENCES

Benjamin, S. G., G. A. Grell, J. M. Brown, T. G. Smirnova, and R. Bleck, 2004a: Mesoscale weather prediction with the RUC hybrid isentropic–terrain-following coordinate model. *Mon. Wea. Rev.*, **132**, 473–494, https://doi.org/10.1175/1520-0493(2004)132<0473:MWPWTR>2.0.CO;2.

——, and Coauthors, 2004b: An hourly assimilation–forecast cycle: The RUC. *Mon. Wea. Rev.*, **132**, 495–518, https://doi.org/10.1175/1520-0493(2004)132<0495:AHACTR>2.0.CO;2.

——, and Coauthors, 2016: A North American hourly assimilation and model forecast cycle: The Rapid Refresh. *Mon. Wea. Rev.*, **144**, 1669–1694, https://doi.org/10.1175/MWR-D-15-0242.1.

Botes, D., J. R. Mecikalski, and G. J. Jedlovec, 2012: Atmospheric Infrared Sounder (AIRS) sounding evaluation and analysis of the pre-convective environment. *J. Geophys. Res.*, **117**, D09205, https://doi.org/10.1029/2011JD016996.

Bothwell, P., J. Hart, and R. Thompson, 2002: An integrated three-dimensional objective analysis scheme in use at the Storm Prediction Center. Preprints, *21st Conf. on Severe Local Storms/19th Conf. on Weather Analysis and Forecasting/15th Conf. on Numerical Weather Prediction.*, San Antonio, TX, Amer. Meteor. Soc., JP3.1, https://ams.confex.com/ams/pdfpapers/47482.pdf.

Coffer, B. E., and M. D. Parker, 2017: Simulated supercells in nontornadic and tornadic VORTEX2 environments. *Mon. Wea. Rev.*, **145**, 149–180, https://doi.org/10.1175/MWR-D-16-0226.1.

——, and ——, 2018: Is there a "tipping point" between simulated nontornadic and tornadic supercells in VORTEX2 environments? *Mon. Wea. Rev.*, **146**, 2667–2693, https://doi.org/10.1175/MWR-D-18-0050.1.

——, ——, R. L. Thompson, B. T. Smith, and R. E. Jewell, 2019: Using near-ground storm relative helicity in supercell tornado forecasting. *Wea. Forecasting*, **34**, 1417–1435, https://doi.org/10.1175/WAF-D-19-0115.1.

——, M. Taszarek, and M. D. Parker, 2020: Near-ground wind profiles of tornadic and nontornadic environments in the United States and Europe from ERA5 reanalyses. *Wea. Forecasting*, **35**, 2621–2638, https://doi.org/10.1175/WAF-D-20-0153.1.

Cohen, A. E., S. M. Cavallo, M. C. Coniglio, H. E. Brooks, and I. L. Jirak, 2017: Evaluation of multiple planetary boundary layer parameterization schemes in southeast U.S. cold season severe thunderstorm environments. *Wea. Forecasting*, **32**, 1857–1884, https://doi.org/10.1175/WAF-D-16-0193.1.

Coniglio, M. C., 2012: Verification of RUC 0–1-h forecasts and SPC mesoscale analyses using VORTEX2 soundings. *Wea. Forecasting*, **27**, 667–683, https://doi.org/10.1175/WAF-D-11-00096.1.

——, and M. D. Parker, 2020: Insights into supercells and their environments from three decades of targeted radiosonde observations. *Mon. Wea. Rev.*, **148**, 4893–4915, https://doi.org/10.1175/MWR-D-20-0105.1.

——, G. S. Romine, D. D. Turner, and R. D. Torn, 2019: Impacts of targeted AERI and Doppler lidar wind retrievals on short-term forecasts of the initiation and early evolution of thunderstorms. *Mon. Wea. Rev.*, **147**, 1149–1170, https://doi.org/10.1175/MWR-D-18-0351.1.

Davies-Jones, R., 2002: Linear and nonlinear propagation of supercell storms. *J. Atmos. Sci.*, **59**, 3178–3205, https://doi.org/10.1175/1520-0469(2003)059<3178:LANPOS>2.0.CO;2.

Esterheld, J. M., and D. J. Giuliano, 2008: Discriminating between tornadic and non-tornadic supercells: A new hodograph technique. *Electron. J. Severe Storms Meteor.*, **3** (2), https://ejssm.org/archives/2008/vol-3-2-2008/.

Evans, C., S. J. Weiss, I. L. Jirak, A. R. Dean, and D. S. Nevius, 2018: An evaluation of paired regional/convection-allowing forecast vertical thermodynamic profiles in warm-season, thunderstorm-supporting environments. *Wea. Forecasting*, **33**, 1547–1566, https://doi.org/10.1175/WAF-D-18-0124.1.

Flournoy, M. D., M. C. Coniglio, E. N. Rasmussen, J. C. Furtado, and B. E. Coffer, 2020: Modes of storm-scale variability and tornado potential in VORTEX2 near-and far-field tornadic environments. *Mon. Wea. Rev.*, **148**, 4185–4207, https://doi.org/10.1175/MWR-D-20-0147.1.

——, ——, and ——, 2021: Examining relationships between environmental conditions and supercell motion in time. *Wea. Forecasting*, **36**, 737–755, https://doi.org/10.1175/WAF-D-20-0192.1.

Fovell, R. G., and A. Gallagher, 2020: Boundary layer and surface verification of the High-Resolution Rapid Refresh, version 3. *Wea. Forecasting*, **35**, 2255–2278, https://doi.org/10.1175/WAF-D-20-0101.1.

Goldacker, N. A., and M. D. Parker, 2021: Low-level updraft intensification in response to environmental wind profiles. *J. Atmos. Sci.*, **78**, 2763–2781, https://doi.org/10.1175/JAS-D-20-0354.1.

Hanft, W., and A. L. Houston, 2018: An observational and modeling study of mesoscale air masses with high theta-E. *Mon. Wea. Rev.*, **146**, 2503–2524, https://doi.org/10.1175/MWR-D-17-0389.1.

Hart, J. A., and A. E. Cohen, 2016: The statistical severe convective risk assessment model. *Wea. Forecasting*, **31**, 1697–1714, https://doi.org/10.1175/WAF-D-16-0004.1.

Hu, M., S. G. Benjamin, T. T. Ladwig, D. C. Dowell, S. S. Weygandt, C. R. Alexander, and J. S. Whitaker, 2017: GSI three-dimensional ensemble–variational hybrid data assimilation using a global ensemble for the regional Rapid Refresh model. *Mon. Wea. Rev.*, **145**, 4205–4225, https://doi.org/10.1175/MWR-D-16-0418.1.

Janjić, Z. I., 2001: Nonsingular implementation of the Mellor–Yamada level 2.5 scheme in the NCEP Meso Model. NCEP Office Note 437, 61 pp., http://www.emc.ncep.noaa.gov/officenotes/newernotes/on437.pdf.

Katona, B., P. Markowski, C. Alexander, and S. Benjamin, 2016: The influence of topography on convective storm environments in the eastern United States as deduced from the HRRR. *Wea. Forecasting*, **31**, 1481–1490, https://doi.org/10.1175/WAF-D-16-0038.1.

Kerr, B. W., and G. L. Darkow, 1996: Storm-relative winds and helicity in the tornadic thunderstorm environment. *Wea. Forecasting*, **11**, 489–505, https://doi.org/10.1175/1520-0434(1996)011<0489:SRWAHI>2.0.CO;2.

Kerr, C. A., D. J. Stensrud, and X. Wang, 2019: Diagnosing convective dependencies on near-storm environments using ensemble sensitivity analyses. *Mon. Wea. Rev.*, **147**, 495–517, https://doi.org/10.1175/MWR-D-18-0140.1.

Kumjian, M. R., and A. V. Ryzhkov, 2012: The impact of size sorting on the polarimetric radar variables. *J. Atmos. Sci.*, **69**, 2042–2060, https://doi.org/10.1175/JAS-D-11-0125.1.

Lawson, J. R., J. S. Kain, N. Yussouf, D. C. Dowell, D. M. Wheatley, K. H. Knopfmeier, and T. A. Jones, 2018: Advancing from convection-allowing NWP to Warn-on-Forecast: Evidence of progress. *Wea. Forecasting*, **33**, 599–607, https://doi.org/10.1175/WAF-D-17-0145.1.

Markowski, P. M., 2020: What is the intrinsic predictability of tornadic supercell thunderstorms? *Mon. Wea. Rev.*, **148**, 3157–3180, https://doi.org/10.1175/MWR-D-20-0076.1.

——, C. Hannon, J. Frame, E. Lancaster, A. Pietrycha, R. Edwards, and R. L. Thompson, 2003: Characteristics of vertical wind profiles near supercells obtained from the Rapid Update Cycle. *Wea. Forecasting*, **18**, 1262–1272, https://doi.org/10.1175/1520-0434(2003)018<1262:COVWPN>2.0.CO;2.

——, N. T. Lis, D. D. Turner, T. R. Lee, and M. S. Buban, 2019: Observations of near-surface vertical wind profiles and vertical momentum fluxes from VORTEX-SE 2017: Comparisons to Monin–Obukhov similarity theory. *Mon. Wea. Rev.*, **147**, 3811–3824, https://doi.org/10.1175/MWR-D-19-0091.1.

Mirocha, J. D., M. D. Simpson, J. D. Fast, L. K. Berg, and R. Baskett, 2016: Investigation of boundary-layer wind predictions during nocturnal low-level jet events using the weather research and forecasting model. *Wind Energy*, **19**, 739–762, https://doi.org/10.1002/we.1862.

Nakanishi, M., and H. Niino, 2009: Development of an improved turbulence closure model for the atmospheric boundary layer. *J. Meteor. Soc. Japan*, **87**, 895–912, https://doi.org/10.2151/jmsj.87.895.

Nixon, C. J., and J. T. Allen, 2021: Anticipating deviant tornado motion using a simple hodograph technique. *Wea. Forecasting*, **36**, 219–235, https://doi.org/10.1175/WAF-D-20-0056.1.

Nowotarski, C. J., and A. A. Jensen, 2013: Classifying proximity soundings with self-organizing maps toward improving supercell and tornado forecasting. *Wea. Forecasting*, **28**, 783–801, https://doi.org/10.1175/WAF-D-12-00125.1.

——, and P. M. Markowski, 2016: Modifications to the near-storm environment induced by simulated supercell thunderstorms. *Mon. Wea. Rev.*, **144**, 273–293, https://doi.org/10.1175/MWR-D-15-0247.1.

Parker, M. D., 2014: Composite VORTEX2 supercell environments from near-storm soundings. *Mon. Wea. Rev.*, **142**, 508–529, https://doi.org/10.1175/MWR-D-13-00167.1.

Peters, J. M., C. J. Nowotarski, J. P. Mulholland, and R. L. Thompson, 2020: The influences of effective inflow layer streamwise vorticity and storm-relative flow on supercell updraft properties. *J. Atmos. Sci.*, **77**, 3033–3057, https://doi.org/10.1175/JAS-D-19-0355.1.

Potvin, C. K., K. L. Elmore, and S. J. Weiss, 2010: Assessing the impacts of proximity sounding criteria on the climatology of significant tornado environments. *Wea. Forecasting*, **25**, 921–930, https://doi.org/10.1175/2010WAF2222368.1.

——, and Coauthors, 2020: Assessing systematic impacts of PBL schemes on storm evolution in the NOAA Warn-on-Forecast System. *Mon. Wea. Rev.*, **148**, 2567–2590, https://doi.org/10.1175/MWR-D-19-0389.1.

Rasmussen, E. N., 2003: Refined supercell and tornado forecast parameters. *Wea. Forecasting*, **18**, 530–535, https://doi.org/10.1175/1520-0434(2003)18<530:RSATFP>2.0.CO;2.

——, and D. O. Blanchard, 1998: A baseline climatology of sounding-derived supercell and tornado forecast parameters. *Wea. Forecasting*, **13**, 1148–1164, https://doi.org/10.1175/1520-0434(1998)013<1148:ABCOSD>2.0.CO;2.

——, S. Richardson, J. M. Straka, P. M. Markowski, and D. O. Blanchard, 2000: The association of significant tornadoes with a baroclinic boundary on 2 June 1995. *Mon. Wea. Rev.*,

128, 174–191, https://doi.org/10.1175/1520-0493(2000)128<0174:TAOSTW>2.0.CO;2.

Smith, B. T., R. L. Thompson, J. S. Grams, C. Broyles, and H. E. Brooks, 2012: Convective modes for significant severe thunderstorms in the contiguous United States. Part I: Storm classification and climatology. *Wea. Forecasting*, **27**, 1114–1135, https://doi.org/10.1175/WAF-D-11-00115.1.

Smith, E. N., J. A. Gibbs, E. Fedorovich, and P. M. Klein, 2018: WRF Model study of the Great Plains low-level jet: Effects of grid spacing and boundary layer parameterization. *J. Appl. Meteor. Climatol.*, **57**, 2375–2397, https://doi.org/10.1175/JAMC-D-17-0361.1.

Taszarek, M., N. Pilguj, J. T. Allen, V. Gensini, H. E. Brooks, and P. Szuster, 2021: Comparison of convective parameters derived from ERA5 and MERRA-2 with rawinsonde data over Europe and North America. *J. Climate*, **34**, 3211–3237, https://doi.org/10.1175/JCLI-D-20-0484.1.

Thompson, R. L., R. Edwards, J. A. Hart, K. L. Elmore, and P. Markowski, 2003: Close proximity soundings within supercell environments obtained from the Rapid Update Cycle. *Wea. Forecasting*, **18**, 1243–1261, https://doi.org/10.1175/1520-0434(2003)018<1243:CPSWSE>2.0.CO;2.

——, C. M. Mead, and R. Edwards, 2007: Effective storm-relative helicity and bulk shear in supercell thunderstorm environments. *Wea. Forecasting*, **22**, 102–115, https://doi.org/10.1175/WAF969.1.

——, B. T. Smith, J. S. Grams, A. R. Dean, and C. Broyles, 2012: Convective modes for significant severe thunderstorms in the contiguous United States. Part II: Supercell and QLCS tornado environments. *Wea. Forecasting*, **27**, 1136–1154, https://doi.org/10.1175/WAF-D-11-00116.1.

Togstad, W. E., J. M. Davies, S. J. Corfidi, D. R. Bright, and A. R. Dean, 2011: Conditional probability estimation for significant tornadoes based on Rapid Update Cycle (RUC) profiles. *Wea. Forecasting*, **26**, 729–743, https://doi.org/10.1175/2011WAF2222440.1.

Trapp, R. J., and J. M. Woznicki, 2017: Convectively induced stabilizations and subsequent recovery with supercell thunderstorms during the Mesoscale Predictability Experiment (MPEX). *Mon. Wea. Rev.*, **145**, 1739–1754, https://doi.org/10.1175/MWR-D-16-0266.1.

Wade, A. R., M. C. Coniglio, and C. L. Ziegler, 2018: Comparison of near-and far-field supercell inflow environments using radiosonde observations. *Mon. Wea. Rev.*, **146**, 2403–2415, https://doi.org/10.1175/MWR-D-17-0276.1.

Wagner, T. J., W. F. Feltz, and S. A. Ackerman, 2008: The temporal evolution of convective indices in storm-producing environments. *Wea. Forecasting*, **23**, 786–794, https://doi.org/10.1175/2008WAF2007046.1.

——, P. M. Klein, and D. D. Turner, 2019: A new generation of ground-based mobile platforms for active and passive profiling of the boundary layer. *Bull. Amer. Meteor. Soc.*, **100**, 137–153, https://doi.org/10.1175/BAMS-D-17-0165.1.

Warren, R. A., H. Richter, H. A. Ramsay, S. T. Siems, and M. J. Manton, 2017: Impact of variations in upper-level shear on simulated supercells. *Mon. Wea. Rev.*, **145**, 2659–2681, https://doi.org/10.1175/MWR-D-16-0412.1.

Weckwerth, T. M., K. J. Weber, D. D. Turner, and S. M. Spuler, 2016: Validation of a water vapor micropulse differential absorption lidar (DIAL). *J. Atmos. Oceanic Technol.*, **33**, 2353–2372, https://doi.org/10.1175/JTECH-D-16-0119.1.

Weisman, M. L., and R. Rotunno, 2000: The use of vertical wind shear versus helicity in interpreting supercell dynamics. *J. Atmos. Sci.*, **57**, 1452–1472, https://doi.org/10.1175/1520-0469(2000)057<1452:TUOVWS>2.0.CO;2.

——, M. Gilmore, and L. Wicker, 1998: The impact of convective storms on their local environment: What is an appropriate ambient sounding? Preprints, *19th Conf. on Severe Local Storms*, Park City, UT, Amer. Meteor. Soc., 238–241.

Weygandt, S., and S. Benjamin, 2007: Radar reflectivity-based initialization of precipitation systems using a diabatic digital filter within the Rapid Update Cycle. *22nd Conf. on Weather Analysis and Forecasting/18th Conf. on Numerical Weather Prediction*, Park City, UT, Amer. Meteor. Soc., 1B.7, https://ams.confex.com/ams/22WAF18NWP/techprogram/paper_124540.htm.

Wilson, M. B., and M. S. Van Den Broeke, 2021: An automated Python algorithm to quantify Z_{DR} Arc and K_{DR}-Z_{DR} separation signatures in supercells. *J. Atmos. Oceanic Technol.*, **38**, 371–386, https://doi.org/10.1175/JTECH-D-20-0056.1.